SCIENTIFIC COMMITTEE
FOURTEENTH REGULAR SESSION

Busan, Republic of Korea
8-16 August 2018

Incorporation of updated growth information within the 2017 WCPO bigeye stock assessment grid, and examination of the sensitivity of estimates to alternative model spatial structures.

WCPFC-SC14-2018/ SA-WP-03

M. T. Vincent, G.M. Pilling and J. Hampton[1]

[1] Oceanic Fisheries Programme, The Pacific Community

Contents

1 Executive Summary

This paper describes the 2018 re-evaluation of bigeye tuna (*Thunnus obesus*) in the western and central Pacific Ocean, incorporating an updated growth curve resulting from analysis of an enhanced set of otolith data, as requested by SC13. The analysis conducted followed the same methodologies as the assessment conducted in 2017 (McKechnie et al., 2017a,b; Tremblay-Boyer et al., 2017). We report the updated results of the uncertainty analysis (model grid) using the axes and weightings from SC13 for consideration in developing management advice. Following the precedent set by McKechnie et al. (2017a), we recommend that management advice be formulated from the results of the structural uncertainty grid. In addition to updating the structural uncertainty grid, we investigated the uncertainty surrounding the spatial structure of the assessment by creating an additional model with the northern boundary of regions 3 and 4 at 15° N, as a one-off sensitivity from two models in the structural uncertainty grid.

Across the range of models in this re-evaluation, the most important factor with respect to the estimated stock status was once again the choice of growth curve ("Updated New" or "Old" growth). The "Updated New growth" model was considerably more optimistic than the "Old growth" model, but was very similar to the "new growth" model presented in 2017. The second key axis in the structural uncertainty grid was whether the northern boundary of regions 3 and 4 was assumed to be at 10° N or 20° N. The former models estimated more optimistic stock status than the latter, though the effect of this assumption was less than for growth. The 10° N model essentially estimates a larger stock size by assigning more stock to the less exploited temperate regions.

The general conclusions of the re-evaluation are as follows:

1. Models that assume the "Updated New growth" estimate depletion to be median$(SB_{recent}/SB_{F=0}) = 0.358$ with an 80% probability interval of 0.295 to 0.412 and all models estimate stock above $20\%SB_{F=0}$

2. All models that assume "Updated New growth" estimate a recent recruitment event that has increased spawning potential in the last several years, and it is expected that for the "Old growth" models these recruits will soon progress into the spawning potential and improve stock status, at least in the short-term.

3. Only the "Old growth" and 20° N boundary models estimate spawning potential to be below $20\%SB_{F=0}$ for all models in the set. These models estimate median$(SB_{recent}/SB_{F=0}) = 0.188$ with an 80% probability interval of 0.123 to 0.275, which is consistent with the structural uncertainty grid of the 2017 assessment.

4. Using a weighting of 3:1 "Updated New : Old growth" as defined by SC13, the recent depletion estimates were median$(SB_{recent}/SB_{F=0}) = 0.334$ with an 80% probability interval of 0.157 to 0.403. Of the 144 weighted runs, 21 (14.58%) estimated $SB_{recent}/SB_{F=0}$ below the LRP of $20\%SB_{F=0}$.

5. Across the weighted grid, exploitation was estimated at median($F_{recent}/F_{\mathrm{MSY}}$) = 0.813 with an 80% probability interval of 0.682 to 1.245, where 32 of the 144 models estimated $F_{recent}/F_{\mathrm{MSY}} > 1$ (22.22%).

Regarding the spatial structure of the model, in particular the northern boundary of regions 3 and 4, the Scientific Committee will have to weigh the spatial information from the various data sources. We investigated the spatial patterns in catch, CPUE and size structure across the key bigeye fisheries here to inform discussions and highlight key data constraints. The results from a model that assumes a northern boundary at 15° N for regions 3 and 4 are compared to models from the structural uncertainty grid for comparable models that assumed a boundary at either 10° N or 20° N. The results from the 15° N model were most similar to the model that assumed a 10° N boundary. Given the similarity of these models, the increased complexity of including multiple spatial structures within a structural uncertainty grid, and concerns regarding data assumptions that may not be valid with 'intermediate' structures, we recommend that the models with the 10° N boundaries be used to develop management advice.

2 Background

The 2017 bigeye tuna assessment (McKechnie et al., 2017a) investigated a range of model assumptions through the structural uncertainty grid approach. The growth axis had the most influence on uncertainty in estimated stock status. The two alternative growth scenarios modelled in the assessment were "new growth" and "old growth". The "new growth" model was based on a growth curve estimated from the analysis of otoliths newly acquired through WCPFC Project 35 (Farley et al., 2017). Conversely, the "old growth" model, as used in the 2014 assessment (Harley et al., 2014), was based on a growth curve constrained by a fixed mean length of the oldest age class of 184 cm. Models that used the "new growth" scenario estimated more optimistic current stock status than models incorporating the "old growth" scenario. SC13 evaluated the growth scenarios and decided to give a weighting of 3:1 in favor of the "new growth" models in the structural uncertainty model grid. However, SC13 noted that the otolith data set used for the estimation of "new growth" was deficient in the number of samples of bigeye tuna larger than 130 cm. As a result, a new project (WCPFC Project 81) was formulated to collect and analyse additional otoliths from larger bigeye tuna in particular. This paper reports the results of incorporating the new growth estimates obtained from the enhanced otolith data into the stock assessment model grid, here referred to as the "Updated New growth" models. Readers should refer to the report of WCPFC Project 81 (SA-WP-01) for more details (Farley et al., 2018).

The second most influential source of uncertainty in the 2017 assessment was associated with the assumed regional structure. Two options were included in the model grid - a boundary of 20° N ("2014 structure") or 10° N ("2017 structure") to separate the tropical regions 3 and 4 from the temperate regions 1 and 2 (Figure 1). SC13 requested further analysis to support the selection of the more appropriate structure. Therefore, this paper also provides analysis of several types of data that might be used in making this choice. In addition, we also provide a one-off sensitivity run using 15° N as the boundary for comparative purposes (Figure 1).

This report should not be considered a new assessment of bigeye tuna, but rather an update with additional data regarding the growth of these fish. We summarize the stock status in terms of reference points (Table 1) adopted by the Western and Central Pacific Fisheries Commission (WCPFC). The methodology used for this re-evaluation is based on the approach of (McKechnie et al., 2017a), which is carried out using the statistical stock assessment software known as MULTIFAN-CL[2] (Fournier et al., 1998; Hampton and Fournier, 2001; Kleiber et al., 2017).

[2] http://www.multifan-cl.org

3 Re-estimation of bigeye status with "Updated New growth" estimates

Within this analysis we address the request from SC13 to re-evaluate bigeye stock status based upon the new growth information developed by WCPFC Project 81. To this end the 36 bigeye "New growth" models in the 2017 grid (Table 2) are re-evaluated using the "Updated New growth" function. The data sources and methodologies described in McKechnie et al. (2017a,b) were identical to those used in this update assessment and those papers should be referred to for full details. Re-evaluation of bigeye growth within the 36 "Updated New growth" models had ramifications on the mean size-at-age, natural mortality (M-at-age), and reproductive output-at-age, which are described below.

3.1 Estimation of "Updated New growth"

Growth was modelled by a von Bertalanffy growth curve following the same assumptions used in 2017 (McKechnie et al., 2017a). Annual and daily age estimates of bigeye tuna from WCPFC Projects 35 and 81 were used to create a dataset, from which a von Bertalanffy (VB) growth estimate was obtained (Farley et al., 2018). Otoliths obtained from fish captured outside the WCPFC Convention Area were excluded from the analysis. Following discussions at the SPC pre-assessment workshop (PAW; Pilling and Brouwer, 2018), the final dataset used to estimate the age-length relationship incorporated annual age estimates that had a readability score of 3 or greater and daily age estimates for fish less than 300 days old or one year depending on the data source (see Farley et al., 2018). When both an annual and daily age estimate were available for a single fish, only the daily age estimate was used in the final dataset. A total of 984 annual age estimates and 58 daily age estimates were used to fit a VB growth model.

A Bayesian analysis with uninformative priors was conducted to estimate the parameters of a VB function. The resulting estimates of L_∞ and k were converted into estimates of L2 and k that were used in the MULTIFAN-CL assessment model. Estimated von Bertalanffy coefficients are as follows: L_∞=156.85 , k=0.303, t_0=-0.69. This translates to MULTIFAN-CL parameters of: L1=38.95, L2=150.70, and k=0.076, where k is specified on a quarterly time scale. The estimated "Updated New growth" curve using this updated data was very different the "Old growth" curve, but was nearly indistinguishable from the 2017 "new growth" model (Figure 2).

Consistent with the assessment conducted in 2017, two growth models were investigated in the assessment process. The "Updated New growth" models used the external k and L2 parameters estimates from the otolith dataset; however, these models estimated the L1 parameter within the MULTIFAN-CL assessment to fit the size frequency data for the small bigeye caught in the Indonesian and Philippines domestic fisheries. As in the 2017 assessment, the "Old growth" model fixed the L2 parameter at 184 cm and estimated additional growth parameters within MULTIFAN-

CL, including L1, k, and the mean length at age for the fish of age 8 quarters or less. Both the "Updated New growth" and the "Old growth" models estimated two length-at-age standard deviation (SD) parameters, a "generic" SD and an "age-dependent" SD (Kleiber et al., 2017).

3.2 Natural Mortality

In the assessment models, natural mortality (M) was fixed at pre-determined age-specific values in an attempt to account for the increase in observed proportions of males with increasing length. Values for M-at-age were calculated using the approach described in McKechnie et al. (2017a), which has also been applied to other tunas in the WCPO and EPO (Harley and Maunder, 2003; Hoyle, 2008; Hoyle and Nichol, 2008). The externally-estimated M-at-age is calculated using observed length-at-age, the observed proportion of males at length, and an assumed average rate of natural mortality. The difference in mean length-at-age between the "Old growth" and "Updated New growth" results in differences in the calculated M-at-age, and these growth-specific mortality vectors were used in the respective assessment models (Figure 3). The M-at-age for the "Updated New growth" was generally higher than the 2017 "new growth" estimates for age classes 12 and older. This difference in the estimated M-at-age can be attributed to a higher standard deviation at length as estimated in the 2017 assessment model.

3.3 Reproductive potential-at-age

Maturity-at-age was calculated from data collected in the WCPO (Farley et al., 2017), and was based on relative reproductive potential rather than the relative biomass of both sexes above the age of female maturity. The reproductive potential of each age class was assumed to be the product of the proportion female at age, the proportion of females mature at age, the spawning frequency at age of mature females, and the fecundity at age per spawning of mature females (Figure 4). The process of estimating reproductive potential-at-age shares some similarities with calculation of M-at-age (Section 3.2) in that the function is calculated at-length and then back-transformed to at-age using an assumed growth function (McKechnie et al., 2017b).

An updated reproductive potential-at-age for the "Updated New growth" models was calculated using the updated growth function, estimated maturity-at-age (from the data of Farley et al., 2017) and updated proportion of females at-age (from Section 3.2). Compared to the "Old growth" estimates of reproductive output at age, the "Updated New growth" function results in a shift in the age at first maturity toward younger fish, and less reduction in the reproductive potential for older age classes (Figure 4). The reproductive output for the "Updated New growth" model resulted in a younger maximum age and larger decline at older ages compared to the 2017 "new growth" model. The difference between the "Updated new growth" and 2017 "new growth" reproductive output-at age can be attributed to the updated estimates of length-at-age and female proportion-at-age.

3.4 Estimation procedures of the uncertainty grid

During the PAW (Pilling and Brouwer, 2018) we reported that slightly better fits could be obtained for some models in the structural uncertainty grid depending on the minimization algorithm used (Davies et al., 2018). For models that assumed "Old growth" in the structural uncertainty grid, we conducted the estimation using different minimization algorithms and selected the model that had the largest likelihood and thus the best fit to the data. For the "Updated New growth" models we ensured that the maximum gradient of the parameters was less than 0.001 using the quasi-Newton minimizer and we are confident that these fits are the best possible.

3.5 Results

Results of the structural uncertainty grid with "Updated New growth" are comparable to those from the 2017 assessment of bigeye (McKechnie et al., 2017a). The results of the structural uncertainty analysis are summarized using a subset of plots to provide advice on key management quantities used by SC13 from the 2017 assessment – time-series plots of fisheries depletion for all models in the grid (Figure 5), boxplots of $F_{recent}/F_{\text{MSY}}$ and $SB_{recent}/SB_{F=0}$ grouped by different levels of each of the five axes of uncertainty (Figure 6), Majuro plots showing the estimates of $F_{recent}/F_{\text{MSY}}$ and $SB_{recent}/SB_{F=0}$ (and $SB_{latest}/SB_{F=0}$ for comparison) across all models in the grid (Figures 7 and 8), and averages and quantiles across the full grid of 72 models for reference points and other quantities of interest (Tables 3 to 5).

Compared to the 2017 assessment results, only small changes in the estimated stock status occurred in the structural uncertainty analysis using the "Updated New growth" models. The growth and regional structure axes once again had significant consequences on the estimated stock status. The general features of the structural uncertainty analysis are as follows:

- All models in the subset of "Updated New growth" models estimate spawning stock depletion to be above the LRP, $20\%SB_{F=0}$, with estimates of depletion $SB_{recent}/SB_{F=0}$ ranging between 0.251 and 0.452 (Table 4).
- The subset of "Old growth" models are substantially more pessimistic (and largely unchanged for the 2017 assessment), with an estimated depletion between 0.09 and 0.31 for the $SB_{recent}/SB_{F=0}$ reference point (Figure 5 and Table 4). Of the 36 models in this subset of the structural uncertainty grid, 21 models estimate $SB_{recent}/SB_{F=0}$ below the LRP, $20\%SB_{F=0}$.
- The second most influential axis was the assumed regional structure where the 10° N models were more optimistic than the 20° N models (Figure 5 panel b and Figure 8 panel a).
- The steepness axis displayed largely predictable results, where the steepness of 0.65 and 0.95 produced more pessimistic and optimistic estimates, respectively, than a steepness of 0.8.

The lower the steepness assumption, the more depleted the stock and the higher the fishing mortality with respect to F_{MSY} (Figure 8 panel b).

– The axes of scaling the likelihood of the size frequency data and overdispersion parameter for the tagging data produced additional uncertainty in the estimated stock status, but their impacts were moderate in comparison to the growth and regional structure axes (Figure 8 panel c and d). No clear trends were discernible between the three levels of size frequency scaling. Down-weighting the tagging data produced generally more pessimistic results, but the differences were not substantial (Figure 5 panel e).

3.5.1 Key differences between Updated New and Old growth models

Consistent with the results of the 2017 assessment, the assumed growth function is one of the major factors that influences the estimated stock status and other model output. The "Updated New growth" and "Old growth" models result in optimistic and pessimistic estimates, respectively. Both models were able to fit the various data components relatively well, including the size frequency data, but the manner in which they do so is quite different. The "Updated New growth" model estimates that the average asymptotic size of the oldest fish is relatively low, but there is substantial variation around size at old ages (Figure 2). Despite this, the model is able to fit even the largest fish caught by the longline (LL) fisheries, although it should be noted that the proportion of fish caught at this size is very low. This model suggests there are very few fish in the population at these sizes and the LL fisheries fully select these fish. This is reflected in the asymptotic selectivity functions estimated for most LL fisheries (Figure 9, red dashed lines).

In contrast, the "Old growth" function sets a much higher asymptotic size for the oldest fish and the estimated variation around the length-at-age is less than for the "Updated New growth" model. This growth model implies that there would be a high number of very large fish in the population in the absence of fishing, but because proportionally few fish at this size are caught, even by the LL fisheries, MULTIFAN-CL estimates that most fish are not reaching this size due to fishing mortality. As a result, the depletion for this model is considerably higher, even in the early years when fishing mortality was relatively low. The assessment model for the "Old growth" also estimates that most LL fisheries do not select for the very old/large fish, which is due to few fish of this size evident in the observed size frequencies (Figure 9, solid black lines). This result conflicts with the usual assumption that the LL fisheries target the old/large fish in the population and brings into question the reliability of this model.

Other important factors influencing the estimates of spawning potential and fisheries depletion between the "Old" and "Updated New growth" models are the values defined for the M-at-age and spawning potential-at-age. For the "Updated New growth" model the M-at-age increases at a younger age compared to the "Old growth" model (Figure 3), which results in estimates of $SB_{F=0}$ that are much larger for the "Updated New growth" model compared to the "Old growth"

model (Tables 4 and 5). For the "Updated New growth" model, the spawning potential function compared to the "Old growth" model shifts the spawning potential function several age-classes younger (Figure 4). This model therefore includes a significant number of extra fish in the spawning population, which is evident in the higher estimates of spawning potential for the "Updated New growth" models.

4 Evaluation of the impacts of Model Spatial Structure

4.1 Background

Stock assessment methods are conducted to represent fish populations and their past dynamics from the observed catch history. These methods are a simplification of reality with the intention of understanding the capability of a population to maintain a relatively stable abundance while being exploited by fisheries. While conducting an assessment, the analyst must define the boundaries of the stock. A stock is defined as all fish belonging to a given species that live within a particular geographic area at a particular time. The boundaries for the stock can be defined for many different reasons. Most often, assessment boundaries are based on political boundaries of the management agency. For bigeye in the WCPO, the perimeter boundaries for the assessment are determined by the jurisdictional boundaries of the WCPFC.

Once the outer stock boundaries are defined, the overall region can be sub-divided. In an ideal situation, boundaries within a stock assessment model would be based on biological characteristics of the species. The purpose of regional boundaries with a stock assessment model is to group fish that experience similar life history characteristics, such as growth and mortality. For example, regions within an assessment model can be based on genetic differences or morphological characteristics of the fish (Cadrin et al., 2004; Grewe et al., 2016). There is some evidence that bigeye may experience different growth between the EPO and the WCPO (Farley et al., 2017, 2018), though samples are currently insufficient to estimate sub-regional growth curves. Additionally, genetic analysis of bigeye tuna in the Pacific Ocean did not show evidence of population subdivision (Grewe and Hampton, 1998). Therefore, creating regional boundaries within the bigeye assessment based on biological characteristics is currently untenable. Furthermore, the MULTIFAN-CL assessment model is not currently capable of accommodating spatial differences in biology where sufficient data are available.

Regional boundaries within an assessment can also be created to separate the stock into groups that experience similar fishing mortality at age. Historical harvest or the return of tagged fish can be used as a proxy of fishing mortality by which to create regional boundaries; the latter proxy can sometimes also be indicative of the level of intermixing between regions. The objective of creating the 9 region assessment model currently used for bigeye and yellowfin tunas was to separate tropical areas where fisheries are present year-round, and temperate areas where fisheries

can be more intermittent (McKechnie et al., 2014). For bigeye, in the WCPO there are large spatial differences in the exploitation of the species as estimated by the regional depletions in McKechnie et al. (2017a). Concurrent with this, encapsulating the spatial distribution of fisheries/gears with comparable selectivity should also be considered.

Another rationale for defining regions in a stock assessment model is to better meet the assumptions associated with tag recovery data. One of the assumptions inherent in analyzing tag-recovery data is that tagged fish are randomly mixed with untagged fish in a region after a defined mixing period. One method to safeguard this assumption is to create many smaller regions. Region 9, the small region to the east of Australia, was added to the assessment model in 2014 to address an issue of insufficient tag mixing in the Coral Sea (McKechnie et al., 2014), which is believed to be a result of more resident behavior of bigeye in the vicinity of land masses and islands. Creating additional regions does necessitate creating a more complex model (i.e., more parameters to estimate), because more fisheries must be defined to operate within each region. Therefore, there is a trade off between creating many regions and the precision of estimates from the assessment model.

The final component in choosing the regional boundaries of a stock assessment is the availability of data. Regional boundaries can only be set where the data are at a resolution that can reliably be separated. In the WCPO there are many limitations to the resolution at which data can be separated. First, the raised catch data used in the assessment are only available at a 5° x 5° resolution. The majority (65%) of the length-composition data are available at a 5° x 5° resolution, though approximately 16% of the size data are at a 10° x 20° or 10° x 10° resolution. Therefore, investigation of different regional structures are limited to at least a 5° resolution.

SC13 noted that the defined regional structure had a notable influence on the results of the 2017 bigeye assessment. Following SC13 recommendations for future research on this aspect of the bigeye assessment, we investigated the spatial component of multiple data sources and compared the estimated population dynamics of three models with differing spatial structures. First, data are analyzed to identify signals that might indicate plausible regional boundaries for the bigeye assessment. Secondly, the impact of modifying the location of the northern boundary of model regions 3 and 4 on model estimates was examined as a 'one-off' sensitivity from the structural uncertainty grid, where the boundary was assumed at 15° N. This model was compared against two models from the structural uncertainty grid, presented above, that assumed a boundary at 10° N or 20° N.

4.2 Data compilation

4.2.1 General characteristics

Longline (LL) fisheries data for the time period 1950 to 2017 were summarized in terms of catch of bigeye in metric tonnes, and catch rate as kilograms of bigeye caught per one hundred hooks

(kg/hhks). The catch data were summed across years to give total catch by 5° x 5° location, while the average across years for each location was calculated for the kg/hhks. For the period 1967 to 2017, the raised total catch of bigeye in metric tonnes and the metric tonnes of bigeye per set was also collected for the purse seine (PS) fishery. The catch for each 5° x 5° location was summed across years and then the log_{10} was calculated to display contrast in the total catch, while the metric tonnes per set was averaged across time for each location. Additionally, length frequency data for the time period 1977 to 2017 with a 5° x 5° spatial sampling design were collated. The average length over time was calculated for each spatial location for the LL and PS fisheries. From these data we investigate the evidence for determining the location of the northern boundary for regions 3 and 4.

4.3 Model description

To examine the sensitivity of MULTIFAN-CL model outputs to a 15° northern boundary of model regions 3 and 4, we performed a one-off sensitivity analysis against two models from the structural uncertainty grid, which assumed a steepness of 0.8, "Updated New growth", the default tagging overdispersion, and the size data likelihood scaling of 20. The only difference between these three models was the assumed location for the northern boundary of regions 3 and 4, either 10° N, 15° N, or 20° N. The 15° N spatial structure model therefore used the same data and model assumptions as described in McKechnie et al. (2017a) and Section 3.1. The available data for the 15° N model are most similar to the 20° N model of the structural uncertainty grid because the model assumes 33 fisheries (McKechnie et al., 2017a). Comparisons are presented among these models for the estimated depletion level, yield, and reproductive potential.

4.4 Results

4.4.1 Spatial investigation of data sources

Catch of bigeye tuna during the most recent decade of the model is most concentrated within 5° of the equator and generally decreases poleward (Figure 10). There is a large decrease in the catch between 10° N and 15° N for the area between 140° E and 170° E. This was a contributing factor to moving the northern regional boundary for regions 3 and 4 to 10° N. Additional support for moving the northern boundary for regions 3 and 4 to 10° N was inferred from the distribution of tag returns (Figures 11 and 12). Two differing conclusions can be inferred from the location of these tag returns. The first possible inference is that fish tagged within the equatorial region generally do not move beyond 10° north or south of the equator, at least for the period that tagged fish were at liberty, 30 to 1701 days (median = 187 days; Schaefer et al., 2015). The other potential inference is that the catch and reporting of tagged fish is concentrated within 10° north or south of the equator.

Both inferences from the tag recapture data suggest that the dynamics, either biologically driven or fishery driven, for bigeye between 10° S and 10° N are different from the rest of the WCPO.

Longline catch per unit effort and total catch The average longline catch per unit effort (kilograms per hundred hooks) showed different spatial patterns from the total catch (Figure 13). A region of high catch per unit effort (CPUE) is observed in the eastern region of the WCPO around 10° – 15° N and CPUE generally decreases moving west and poleward. There is also a moderately high level of CPUE to the north and south of Hawaii. Areas with the largest total catch are not always associated with high CPUE. High longline catch occurred in the following locations: to the east of Japan, between the equator and 10° N east of 130° E, at 15° N east of 170° E, and in the southeast corner of region 4. Only the region of high CPUE at 15° N is aligned with a region of high catch.

Purse seine catch per unit effort and total catch Areas of high catch per unit effort of bigeye (i.e., metric tonnes per set) for the purse seine fishery are nearly inversely related to the total catch within the equatorial region (Figure 14). The highest CPUE for the purse seine fishery occurs in the eastern portion of region 4, below the 10° N boundary. The greatest catch density occurs within region 8 and the 5° x 5° cells that border this region, within region 3. The catch of bigeye decreases exponentially poleward to the point of virtually no catch north or south of 20°, with the exception of catch in region 1 to the east of Japan. The amount of total catch of bigeye over the period 1967 to 2017 north of 10° N and east of 170° E is only 145 metric tonnes compared to nearly 450,000 metric tonnes of total catch in the rest of region 4. Similarly, around a total of 600 metric tonnes of bigeye have been caught in the region between 10° N – 20 ° N and 140° – 170° E, while over a million metric tonnes have been caught in regions 3 and 8. Therefore, a negligible amount of bigeye catch has occurred between 10° N and 20° N east of 140° E and setting the boundary at 10° N is reasonable on that basis.

Average Length The average length from the 5° x 5° sampling is very informative about the difference in size at catch for the purse seine and the LL fisheries (Figure 15). For the longline fishery, sampled bigeye average lengths ranged between 89 cm and 192 cm and on average, across the time period and spatial extent, were 120 cm long. Bigeye sampled from the purse seine fishery were on average, across the time period and location, 60 cm long and were between 24 cm and 100 cm. Therefore, the size at catch for the LL fishery is twice that of the purse seine fishery. This dynamic should be accounted for in the assessment model by creating regional boundaries that reflect the spatial extent of the purse seine catch. Therefore, the average length of bigeye provides further evidence for setting the northern boundary of regions 3 and 4 at 10° N.

The spatial pattern of the average length captured by the LL fishery is almost the opposite of the pattern displayed by the average length for all fisheries (Figure 15, panel a). The largest length

of bigeye samples from the LL fishery occur near the equator between 5° S and 15° N. Relatively smaller fish captured by the LL fishery occur in the more poleward extents of the WCPO. However, there are some very large bigeye captured at the spatial margins of the observed length frequency data, but the number of size samples from these location are typically less than 5. Length samples were most commonly obtained to the east of Indonesia and on the boundary between regions 3 and 4, with samples around Hawaii also relatively common.

The observed length data sampled from the purse seine fishery are almost entirely contained within 15° S and 10° N (Figure 15, panel b). The smallest bigeye captured by the purse seine fishery generally occurred at 10° N and fish captured below this were larger on average. The locations of greater frequency of observed lengths are consistent with the locations of higher catch by the purse seine fishery (Figure 10).

4.4.2 Comparison to other spatial structures

The population dynamics model that assumed a northern boundary for regions 3 and 4 at 15° N estimated stock status that was closer to estimates from the 10° N model than the 20° N model. The reference points estimated by the one-off sensitivity model and the two models from the structural uncertainty grid are presented in Table 6.

Comparing the trajectories of estimated dynamic depletion (Figure 16) for models with three different spatial structures, the 15° N model was most similar to the 10° N. The 10° N and 15° N models estimate dynamic depletion nearly identically for the period 1952 to 2000 and then after the 15° N model estimates slightly more depletion. Estimates of spawning potential were also most similar between the 15° N and 10° N, where the 15° N estimated slightly higher spawning potential earlier in the time series (Figure 17). The yield curves relative to current effort for the three models show that the 15° N model has the largest maximum yield but declines more quickly with greater fishing compared to the 10° N model (Figure 18). The maximum yield for the 20° N model is much lower than estimates from the 10° N and 15° N models.

Estimates of stock status from the 15° N were most similar to the 10° N model though the number of fisheries was the same as the 20° N model. The difference in stock-status appears to be driven by the fit to the standardized CPUE for the LL fishery in region 4; the fit for the 15° N model more closely resembles the fit by the 10° N model (Figure 19). Though the 15° N model still separates the US longline into two fisheries, the majority of the size composition data is located in region 2 for the 15° N and thus matches the 10° N more than the 20° N model. Finally, regional contribution of total biomass by weight from the 15° N model are most similar to the 10° N model and appear to have a large influence on the estimated scale of the population (Figure 20).

5 Discussion and conclusions

5.1 Changes to the previous assessment

The re-analysis of the 2017 assessment incorporated the latest data on WCPO bigeye growth arising from WCPFC Project 81. Compared to the results of the 2017 assessment, this information resulted in only minor changes regarding the growth function and other quantities that were dependent on the length-at-age relationship (Figure 2). The resulting estimates of stock status from the structural uncertainty grid were nearly identical to the estimates from the 2017 assessment. Uncertainty in stock-status estimates were again largest for the structural uncertainty axis of growth and to a lesser extent the spatial structure. Estimates of depletion and reference points were generally consistent with estimates from the 2017 assessment.

5.2 Investigation of growth

The Scientific Committee must once again assess the evidence to support each of the two alternative growth options, as this will affect management recommendations formulated from this assessment. The "Old growth" model excludes the most current information regarding the age at length of bigeye. The Scientific Committee will need to assess the support for excluding this data source from the assessment model.

If recommendations are made based solely on models using the "Updated New growth" function, then the bigeye stock in the WCPO appears to be not overfished although several model runs are at the designated boundary of overfishing. If models with the "Old growth" are also considered for formulating recommendations, then estimates of stock status are less definitive. The old growth models with the 10° N regional structure are more optimistic than the 20° N assessment results. Most model runs in the "Old growth" and 10° N category terminate around or above the limit reference point, $20\%SB_{F=0}$. In contrast, models with the "Old growth" and 20° N regional structure are more pessimistic and are generally more consistent with 2014 assessment results. All models in this sub-set of the structural uncertainty grid terminate below the limit reference point.

If the weighting of three "Updated New growth" models to one "Old growth" models are considered for formulating recommendations, then estimates of stock status are generally consistent with the advice of SC13.

The collection of additional otoliths from large bigeye tuna to assist the estimation of the von Bertalanffy growth curve did not significantly impact the estimated growth curve or the assessed status of the stock compared to the 2017 assessment. The additional age estimates from larger individuals have further reduced the uncertainty surrounding the growth curve. However, MULTIFAN-CL had difficulty fitting the smallest size fish observed in the size frequency data, which were harvested

in region 7. Given the different methodologies used to age fish within the WCPO and EPO (e.g., annual versus daily ageing), the following recommendations are made:

- Collaboration with the IATTC to analyze bigeye growth from otolith and tagging data collected across the entire Pacific, to better characterize the apparent regional difference in growth between the WCPO and EPO, and possible environmental determinants of such differences.
- Analyzing the same otoliths by different laboratories, to build confidence in ageing estimates and to estimate ageing error.
- Continued development of a high-confidence tagging dataset for growth analysis, with particular focus on larger bigeye tuna and events with reliable measurements at release. Such data would assist with the validation of the age estimates of large bigeye in the WCPO, and could potentially be incorporated directly into the assessment model as an additional data set. However, a reliable measurement of both length at release and recapture are necessary to accurately estimate incremental growth.
- Collect otoliths of very small bigeye that are captured by the Indonesian, Vietnamese, and Philippines domestic fisheries in region 7 and estimate age through daily ring counts to aid the estimation of the L1 parameter within the assessment model.

5.3 Main re-evaluation conclusions

The main conclusions of the current re-evaluation of bigeye status are similar to the 2017 assessment (McKechnie et al., 2017a). The Scientific Committee will have to assess the plausibility of the different models in the structural uncertainty grid, particularly four groups of models resulting from different combinations of the "Updated New" and "Old growth", and the 10° N and 20° N regional structure. To this end, we summarize the general conclusions of this assessment as follows:

- Models that assume the "Updated New growth" estimate depletion to be median($SB_{recent}/SB_{F=0}$) = 0.358 with an 80% probability interval of 0.295 to 0.412 and all models estimate stock above 20%$SB_{F=0}$.
- All models with the "Updated New growth" function estimate a significant recent recruitment event that has increased spawning potential in the last several years; it is expected that these recruitments will soon progress into the spawning potential for the "Old growth" models and increase stock status, at least in the short-term.
- Of the four sets of models in the structural uncertainty grid (the combinations of the "Old / Updated New growth" and the 10° / 20° N regional structure), only the "Old growth" 20° N models estimate spawning potential to be below 20%$SB_{F=0}$ for all models in the set.

These models estimate $SB_{recent}/SB_{F=0}$ to be between 0.095 and 0.195, which is similar to the structural uncertainty grid of the 2017 assessment.

- A substantial decline in bigeye abundance was estimated by all models in the assessment; estimates of depletion, both relative to estimates earlier in the assessment period and estimates in the absence of fishing, are substantial and appear to be ongoing, at least on a multi-year scale.
- Using a weighting of 3:1 "Updated New : Old growth", the recent depletion estimated median$(SB_{recent}/SB_{F=0}) = 0.334$ with an 80% probability interval of 0.157 to 0.403. Of the 144 weighted runs, 21 (14.58%) estimated $SB_{recent}/SB_{F=0}$ below the LRP of $20\%SB_{F=0}$.
- Across the weighted grid, median$(F_{recent}/F_{\text{MSY}}) = 0.813$ with an 80% probability interval of 0.682 to 1.245, where 32 of the 144 models estimated $F_{recent}/F_{\text{MSY}} > 1$ (22.22%).

5.4 Structural uncertainty

A challenge when developing the spatial structure of WCPO stock assessment models is the relatively limited, and potentially conflicting, information from which precise boundaries can be inferred. Informed decisions must be taken, and where necessary the sensitivity of estimates to changes examined. However, the increased time required to create the necessary alternative input files for different spatial structures makes it preferable to select a single structure, particularly where the results of the model are insensitive.

Creating a structural uncertainty grid that assumes multiple spatial structures is more difficult than just drawing lines on a map. All data sources must be reconfigured with each spatial structure investigated, such as the fisheries definitions, catch, tag releases and recoveries, CPUE indices, regional weighting, and size composition data. This greatly increases the complexity of creating the structural uncertainty grid and increases the difficulty and time to complete an assessment in this manner.

For the 15° N model, most data sources were straightforward to create following the methodology presented in McKechnie et al. (2017a). However, the size composition data were more complicated to extract. The majority of the size composition data were sampled in a 5° x 5° spatial structure, but almost a fifth of the size frequency data were collected from a 10° x 10° or 10° x 20° sampling design. The frequency data from these two sampling designs needed to be separated between two regions because the northern boundaries for regions 3 and 4 were assumed at 15° N. To separate these data we assumed that half of the samples were collected in each region, following the precedent used to separate the 10° x 20° samples along the 100° E, 170° E, and 150° W boundaries (McKechnie et al., 2017a,b). This assumption may be questionable for the 15° N model given that the catch and size frequency change between these two latitudes. Therefore, either the 10° N or 20° N model is preferable to the 15° N model.

The analysis of data presented here provides further support to the 10° N boundary, rather than the historical boundary at 20° N. In turn, while some data suggest a 15° N boundary is potentially valid, the impact on model results appears limited.

Acknowledgments

We thank the various fisheries agencies for the provision of the catch, effort and size frequency data used in this analysis.

References

Cadrin, S., Friedland, K., and Waldman, J., editors (2004). *Stock identification methods: applications in fishery science*. Elsevier Academic Press, Burlington, Mass.

Davies, N., Fournier, D., Takeuchi, Y., Bouye, F., and Hampton, J. (2018). Developments in the MULTIFAN-CL software 2017-2018. Technical Report WCPFC-SC-2018/SA-IP-02, Busan, Korea, 8–16 August 2018.

Farley, J., Eveson, P., Krusic-Golub, K., Clear, N., Sanchez, C., Roupsard, F., Satoh, K., Smith, N., and Hampton, J. (2018). Project 81: Update on age and growth of bigeye tuna in the western and central pacific ocean. Technical Report WCPFC-SC14-2018/SA-WP-01, Busan, Korea, 8–16 August 2018.

Farley, J., Eveson, P., Krusic-Golub, K., Sanchez, C., Roupsard, F., McKechnie, S., Nichol, S., Leroy, B., Smith, N., and Chang, S.-K. (2017). Age, growth and maturity of bigeye tuna in the western and central Pacific Ocean. WCPFC-SC13-2017/SA-WP-01, Rarotonga, Cook Islands, 9–17 August 2017.

Fournier, D., Hampton, J., and Sibert, J. (1998). MULTIFAN-CL: a length-based, age-structured model for fisheries stock assessment, with application to South Pacific albacore, *Thunnus alalunga*. *Canadian Journal of Fisheries and Aquatic Sciences*, 55:2105–2116.

Grewe, P. and Hampton, J. (1998). An assessment of bigeye (thunnus obesus) population structure in the pacific ocean based on mitochondrial dna and dna microsatellite analysis. Technical report, JIMAR Contribution 98-330.

Grewe, P., Irianto, H., Proctor, C., Adam, M., Jauhary, A., Schaefer, K., Itano, D., Killian, A., and Davies, C. (2016). Population structure and provenance of tropical tunas: recent results from high throughput genotyping and potential implications for monitoring and assessment. WCPFC-2016-SC12/SA-WP-01, CSIRO, Stones Hotel, Kuta, Bali, Indonesia.

Hampton, J. and Fournier, D. (2001). A spatially-disaggregated, length-based, age-structured population model of yellowfin tuna (*Thunnus albacares*) in the western and central Pacific Ocean. *Marine and Freshwater Research*, 52:937–963.

Harley, S. J., Davies, N., Hampton, J., and McKechnie, S. (2014). Stock assessment of bigeye tuna in the Western and Central Pacific Ocean. WCPFC-SC10-2014/SA-WP-01, Majuro, Republic of the Marshall Islands, 6–14 August 2014.

Harley, S. J. and Maunder, M. N. (2003). A simple model for age-structured natural mortality based on changes in sex ratios. Technical Report SAR-4-01, Inter-American Tropical Tuna Commission, La Jolla, California, USA, 19–21 May 2003.

Hoyle, S. and Nichol, S. (2008). Sensitivity of bigeye stock assessment to alternative biological and reporductive assumptions. WCPFC-SC4-2008/ME-WP-01, Port Moresby, Papua New Guinea, 11–22 August 2008.

Hoyle, S. D. (2008). Adjusted biological parameters and spawning biomass calculations for south Pacific albacore tuna, and their implications for stock assessments. WCPFC-SC4-2008/ME-WP-02, Port Moresby, Papua New Guinea, 11–22 August 2008.

Kleiber, P., Fournier, D., Hampton, J., Davies, N., Bouye, F., and Hoyle, S. (2017). *MULTIFAN-CL User's Guide*. http://www.multifan-cl.org/.

McKechnie, S., Harley, S. J., Davies, N., Rice, J., Hampton, J., and Berger, A. (2014). Basis for regional structures used in the 2014 tropical tuna assessments, including regional weights. WCPFC-SC10-2014/SA-IP-02, Majuro, Republic of the Marshall Islands, 6–14 August 2014.

McKechnie, S., Pilling, G., and Hampton, J. (2017a). Stock assessment of bigeye tuna in the western and central Pacific Ocean. WCPFC-SC13-2017/SA-WP-05, Rarotonga, Cook Islands, 9–17 August 2017.

McKechnie, S., Tremblay-Boyer, L., and Pilling, G. (2017b). Background analyses for the 2017 stock assessments of bigeye and yellowfin tuna in the western and central Pacific Ocean. WCPFC-SC13-2017/SA-IP-06, Rarotonga, Cook Islands, 9–17 August 2017.

Pilling, G. M. and Brouwer, S. (2018). Report from the spc pre-assessment workshop, noumea, april 2018. Technical Report WCPFC-SC14-2018/SA-IP-01, Busan, Korea, 8–16 August 2018.

Schaefer, K., Fuller, D., Hampton, J., Caillot, S., Leroy, B., and Itano, D. (2015). Movements, dispersion, and mixing of bigeye tuna (*Thunnus obesus*) tagged and released in the equatorial Central Pacific Ocean, with conventional and archival tags. *Fisheries Research*, 161:336–355.

Tremblay-Boyer, L., McKechnie, S., Pilling, G., and Hampton, J. (2017). Stock assessment of yellowfin tuna in the Western and Central Pacific Ocean. WCPFC-SC13-2017/SA-WP-06, Rarotonga, Cook Islands, 9–17 August 2017.

6 Tables

Table 1: Description of symbols used in the yield and stock status analyses. For the purpose of this assessment, "recent" for spawning potential the is the average over the period 2012–2015, while "recent" for fishing mortality is the average over the period 2011–2014 and "latest" is 2015.

Symbol	Description
C_{latest}	Catch in the last year of the assessment (2015)
F_{recent}	Average fishing mortality-at-age for a recent period (2011–2014)
$Y_{F_{recent}}$	Equilibrium yield at average fishing mortality for a recent period (2011–2014)
f_{mult}	Fishing mortality multiplier at maximum sustainable yield (MSY)
F_{MSY}	Fishing mortality-at-age producing the maximum sustainable yield (MSY)
MSY	Equilibrium yield at F_{MSY}
$F_{recent}/F_{\text{MSY}}$	Average fishing mortality-at-age for a recent period (2011–2014) relative to F_{MSY}
SB_0	Equilibrium unexploited spawning potential
SB_{latest}	Spawning potential in the latest time period (2015)
SB_{recent}	Spawning potential for a recent period (2012–2015)
$SB_{F=0}$	Average spawning potential predicted in the absence of fishing for the period 2005–2014
SB_{MSY}	Spawning potential that will produce the maximum sustainable yield (MSY)
SB_{MSY}/SB_0	Spawning potential that produces maximum sustainable yield (MSY) relative to the average Spawning potential predicted to occur in the absence of fishing for the period 2005–2014
$SB_{MSY}/SB_{F=0}$	Spawning potential that produces the maximum sustainable yield (MSY) relative to the equilibrium unexploited spawning potential
SB_{latest}/SB_0	Spawning potential in the latest time period (2015) relative to the equilibrium unexploited spawning potential
$SB_{latest}/SB_{F=0}$	Spawning potential in the latest time period (2015) relative to the average spawning potential predicted to occur in the absence of fishing for the period 2005–2014
$SB_{latest}/SB_{\text{MSY}}$	Spawning potential in the latest time period (2015) relative to that which will produce the maximum sustainable yield (MSY)
$SB_{recent}/SB_{F=0}$	Spawning potential for a recent period (2012–2015) relative to the average spawning biomass predicted to occur in the absence of fishing for the period 2005–2014
$SB_{recent}/SB_{\text{MSY}}$	Spawning potential for a recent period (2012–2015) relative to the spawning potential that produces maximum sustainable yield (MSY)
$20\%SB_{F=0}$	WCPFC adopted limit reference point – 20% of spawning potential in the absence of fishing average over years $t-10$ to $t-1$ (2005–2014)

Table 2: Description of the structural sensitivity grid used to characterise uncertainty in the assessment (from McKechnie et al., 2017a).

Axis	Levels	Option
Steepness	3	0.65, 0.80, or 0.95
Growth	2	"Updated New growth" L2 = 151, "Old growth" L2 = 184
Tagging overdispersion	2	Default level, Fixed (moderate) level
Size frequency weighting	3	Sample sizes divided by 10, 20, or 50
Regional structure	2	10° N boundary, 20° N boundary

Table 3: Summary of reference points over all 72 models in the structural uncertainty grid where the models using the "Updated New growth" function are given three times the weighting of the models using the "Old growth" function.

	Mean	Median	Min	10	90	Max
C_{latest}	152591	152806	143553	148905	156160	157726
$Y_{F_{recent}}$	150995	150780	117360	135148	169888	172280
f_{mult}	1.188	1.230	0.613	0.803	1.467	1.690
F_{MSY}	0.049	0.049	0.035	0.044	0.054	0.056
MSY	155543	156240	123440	137232	173016	180120
$F_{recent}/F_{\text{MSY}}$	0.887	0.813	0.592	0.682	1.245	1.632
SB_0	1609660	1614000	1026000	1297000	1929700	2085000
$SB_{F=0}$	1810313	1827590	1342229	1579140	2032633	2139644
SB_{MSY}	439774	432900	225800	310210	576610	614200
SB_{MSY}/SB_0	0.271	0.273	0.217	0.239	0.299	0.302
$SB_{MSY}/SB_{F=0}$	0.241	0.244	0.167	0.189	0.280	0.287
SB_{latest}/SB_0	0.399	0.435	0.130	0.204	0.512	0.568
$SB_{latest}/SB_{F=0}$	0.358	0.390	0.096	0.158	0.470	0.526
$SB_{latest}/SB_{\text{MSY}}$	1.466	1.544	0.503	0.870	1.926	2.187
$SB_{recent}/SB_{F=0}$	0.312	0.334	0.094	0.157	0.403	0.452
$SB_{recent}/SB_{\text{MSY}}$	1.285	1.329	0.494	0.858	1.650	1.879

Table 4: Summary of reference points over the 36 models in the structural uncertainty grid within the subset of "Updated New growth" models (both 10° N and 20° N regions).

	Mean	Median	Min	10	90	Max
C_{latest}	152148	151846	148888	148936	154971	155577
$Y_{F_{recent}}$	154180	153220	133120	141140	170720	172280
f_{mult}	1.291	1.301	0.946	1.075	1.499	1.690
F_{MSY}	0.050	0.049	0.044	0.045	0.054	0.056
MSY	158551	159020	133520	143040	173880	180120
$F_{recent}/F_{\text{MSY}}$	0.789	0.768	0.592	0.667	0.931	1.058
SB_0	1674833	1675500	1261000	1415500	1941000	2085000
$SB_{F=0}$	1841609	1858775	1509007	1632014	2043108	2139644
SB_{MSY}	471956	476050	340700	386600	577400	614200
SB_{MSY}/SB_0	0.281	0.280	0.260	0.262	0.300	0.302
$SB_{MSY}/SB_{F=0}$	0.255	0.255	0.226	0.235	0.280	0.287
SB_{latest}/SB_0	0.456	0.456	0.346	0.392	0.523	0.568
$SB_{latest}/SB_{F=0}$	0.414	0.420	0.298	0.351	0.480	0.526
$SB_{latest}/SB_{\text{MSY}}$	1.633	1.624	1.146	1.306	1.933	2.187
$SB_{recent}/SB_{F=0}$	0.353	0.358	0.251	0.295	0.412	0.452
$SB_{recent}/SB_{\text{MSY}}$	1.394	1.377	0.963	1.117	1.659	1.879

Table 5: Summary of reference points over the 36 models in the structural uncertainty grid within the subset of all "Old growth" models (both 10° N and 20° N regions.

	Mean	Median	Min	10	90	Max
C_{latest}	153918	155968	143553	144708	157298	157726
$Y_{F_{recent}}$	141441	142000	117360	125760	158860	168600
f_{mult}	0.880	0.874	0.613	0.683	1.109	1.218
F_{MSY}	0.046	0.045	0.035	0.040	0.053	0.055
MSY	146519	144360	123440	129340	164200	168800
$F_{recent}/F_{\text{MSY}}$	1.181	1.144	0.821	0.902	1.466	1.632
SB_0	1414139	1426500	1026000	1099000	1684500	1921000
$SB_{F=0}$	1716424	1698665	1342229	1424942	1991569	2042628
SB_{MSY}	343231	338100	225800	238650	430900	511400
SB_{MSY}/SB_0	0.241	0.239	0.217	0.219	0.261	0.266
$SB_{MSY}/SB_{F=0}$	0.198	0.195	0.167	0.168	0.225	0.256
SB_{latest}/SB_0	0.230	0.228	0.130	0.164	0.306	0.335
$SB_{latest}/SB_{F=0}$	0.192	0.190	0.096	0.125	0.271	0.311
$SB_{latest}/SB_{\text{MSY}}$	0.965	0.903	0.503	0.649	1.355	1.479
$SB_{recent}/SB_{F=0}$	0.190	0.188	0.094	0.123	0.275	0.313
$SB_{recent}/SB_{\text{MSY}}$	0.956	0.896	0.494	0.635	1.335	1.488

Table 6: Summary of reference points for a one-off sensitivity model and two models from the structural uncertainty grid that assume "Updated New growth", steepness of 0.8, size weighting of 20, and default tag weighting. The difference between the model was the location of the northern boundary for regions 3 and 4, either 10° N, 15° N, or 20° N.

	10° N	15° N	20° N
C_{latest}	155476	152776	151384
$Y_{F_{recent}}$	157920	161560	151360
f_{mult}	1.568	1.508	1.227
F_{MSY}	0.048	0.049	0.051
MSY	169720	171520	153680
$F_{recent}/F_{\text{MSY}}$	0.638	0.663	0.815
SB_0	1880000	1851000	1556000
$SB_{F=0}$	1992074	1929938	1739016
SB_{MSY}	519200	512700	440000
SB_{MSY}/SB_0	0.276	0.277	0.283
$SB_{MSY}/SB_{F=0}$	0.261	0.266	0.253
SB_{latest}/SB_0	0.533	0.495	0.442
$SB_{latest}/SB_{F=0}$	0.503	0.474	0.395
$SB_{latest}/SB_{\text{MSY}}$	1.931	1.785	1.562
$SB_{recent}/SB_{F=0}$	0.432	0.405	0.334
$SB_{recent}/SB_{\text{MSY}}$	1.659	1.524	1.322

7 Figures

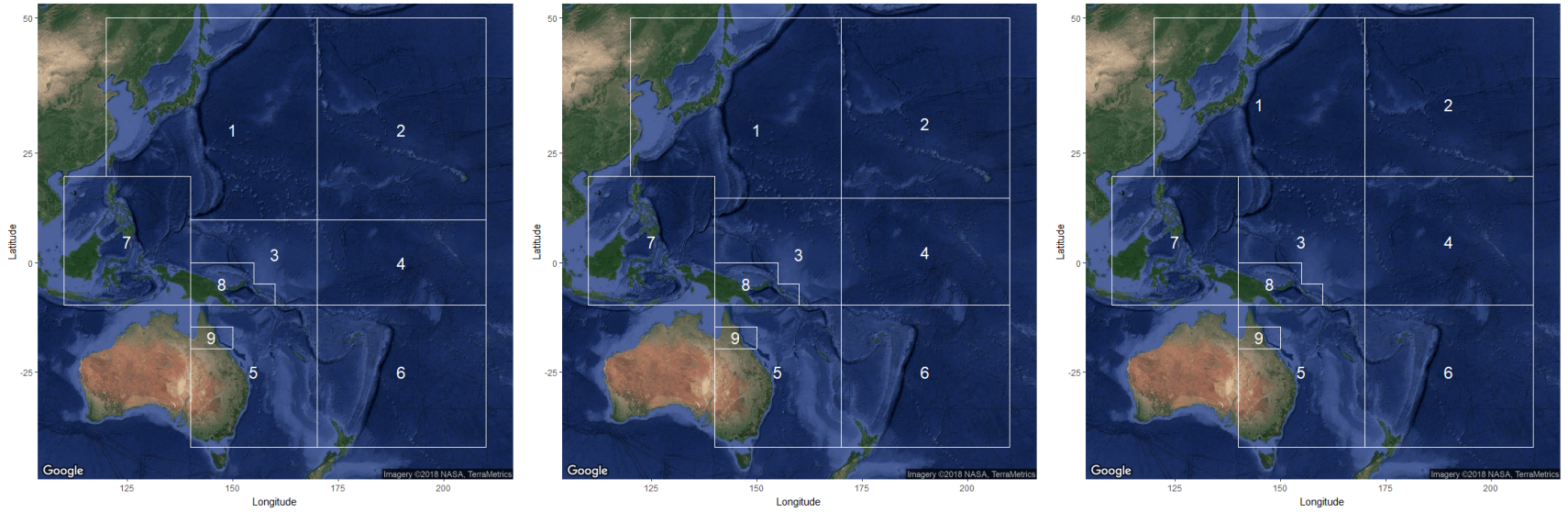

(a) 10° N model (b) 15° N model (c) 20° N model

Figure 1: The geographical area covered by the stock assessment and the boundaries for the 9 regions for the (a) 10° N regional structure, (b) 15° N regional structure, and (c) 20° N regional structure.

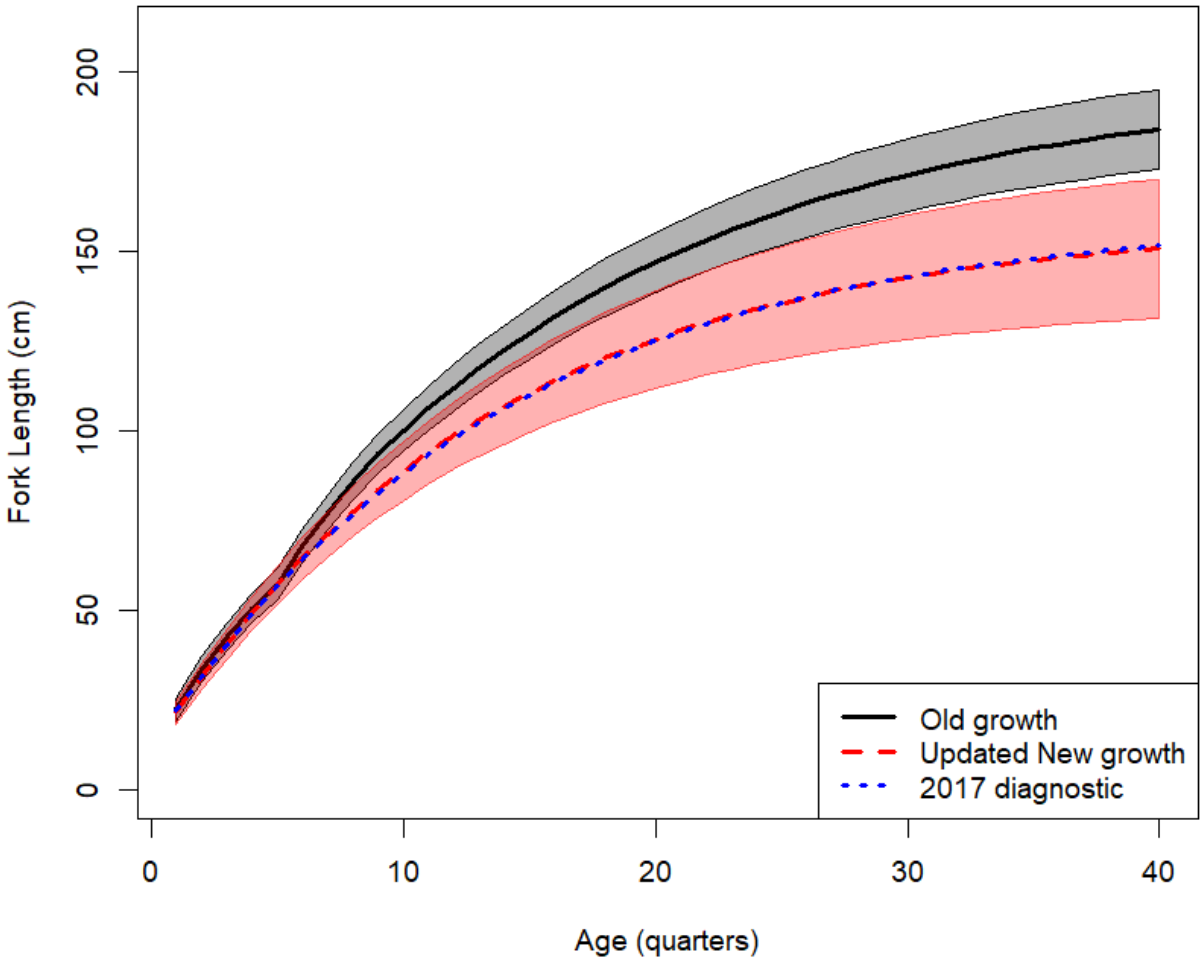

Figure 2: Estimated von Bertalanffy curves for the "Updated New growth" (red dashed line) and "Old growth" (black solid line) assessment models in the structural uncertainty grid and the diagnostic case model from 2017 (blue dotted line), where the models assumed overdisperision at the default value, weighting of the size composition of 20, and the 10° N spatial structure. The lines represent the estimated mean fork length (cm) at-age and the regions represent the length-at-age within one standard deviation of the mean.

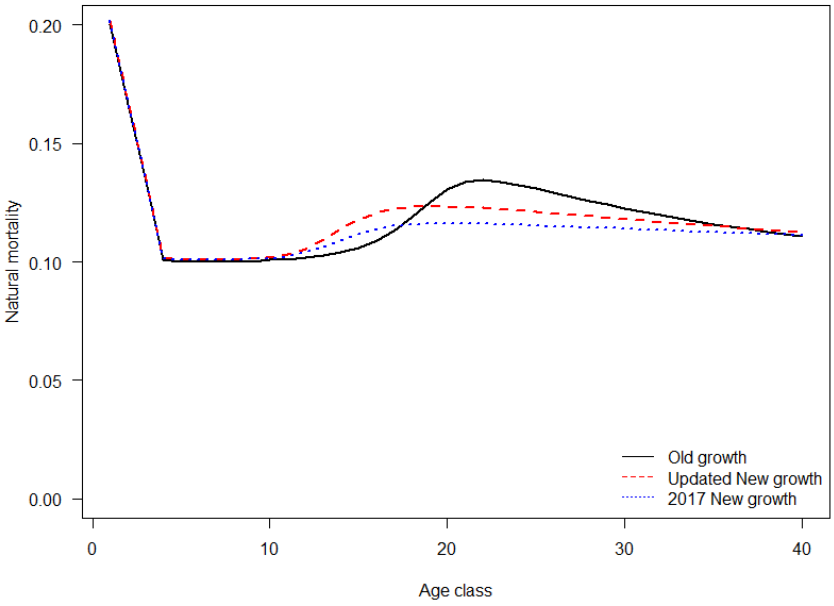

Figure 3: Quarterly natural mortality-at-age as used in the "Old growth" (solid black line), "Updated New growth" (red dashed line), and 2017 "new growth" (dotted blue line) models.

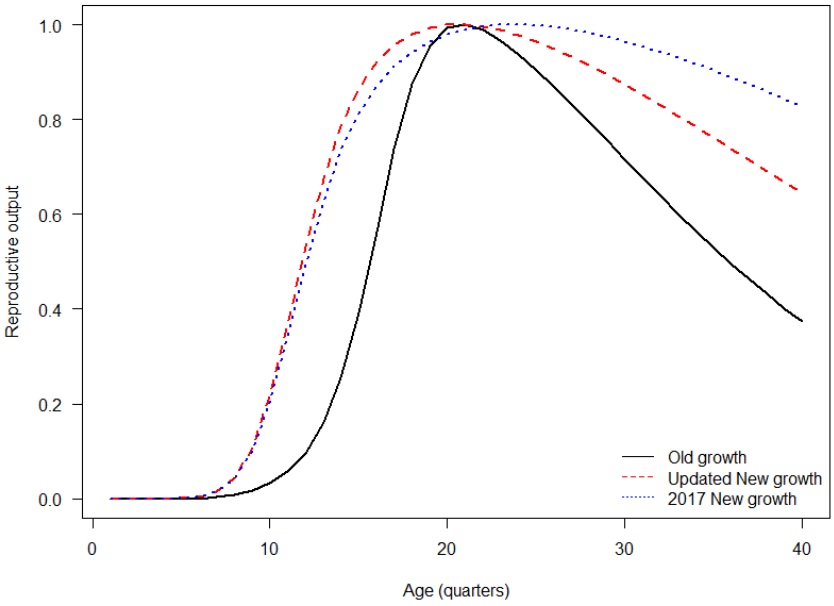

Figure 4: Maturity-at-age as used in the "Old growth" (solid black line), "Updated New growth" (red dashed line), and 2017 "new growth" (dotted blue line) models.

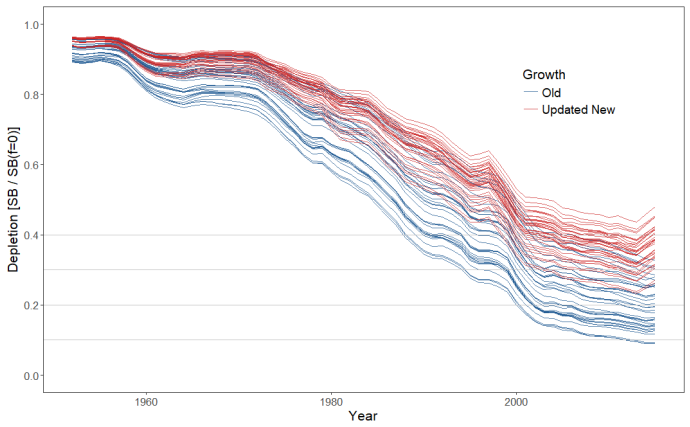

(a) Old and Updated New growth

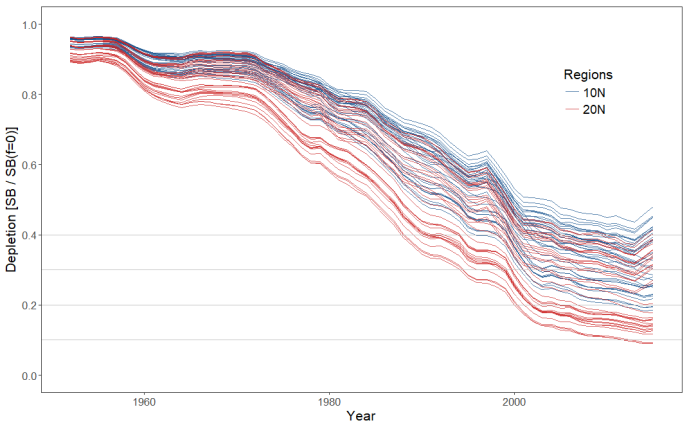

(b) 20° N and 10° N regions

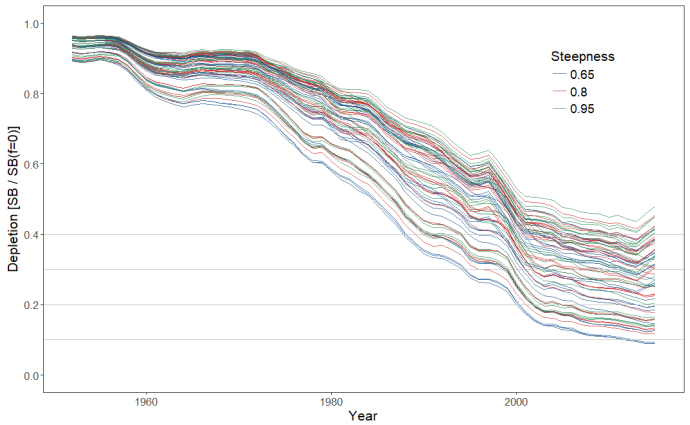

(c) Steepness

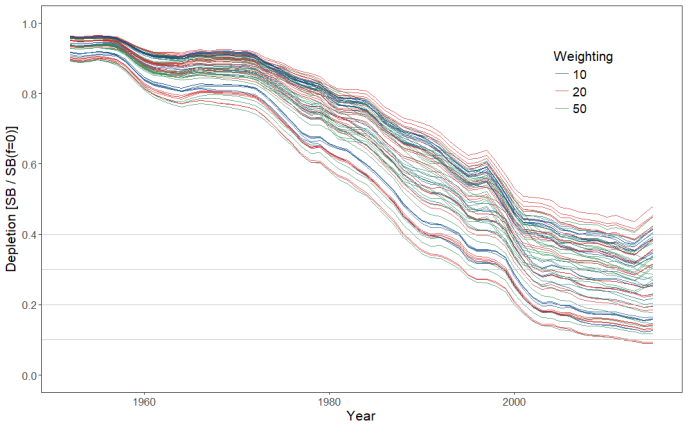

(d) Weighting of size data

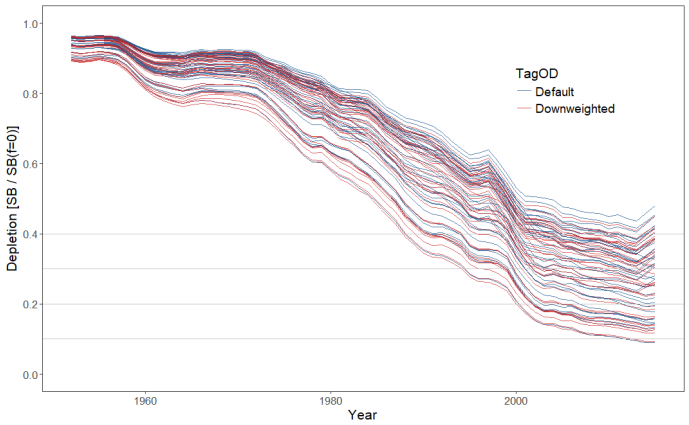

(e) Weighting of tagging data

Figure 5: Plots showing the trajectories of fishing depletion (of spawning potential) for model runs included in the structural uncertainty grid (see McKechnie et al. (2017a) for details of the structure of the grid models). The five panels show the models separated on the basis of the five axes used in the grid, with the color denoting the level within the axes for each model.

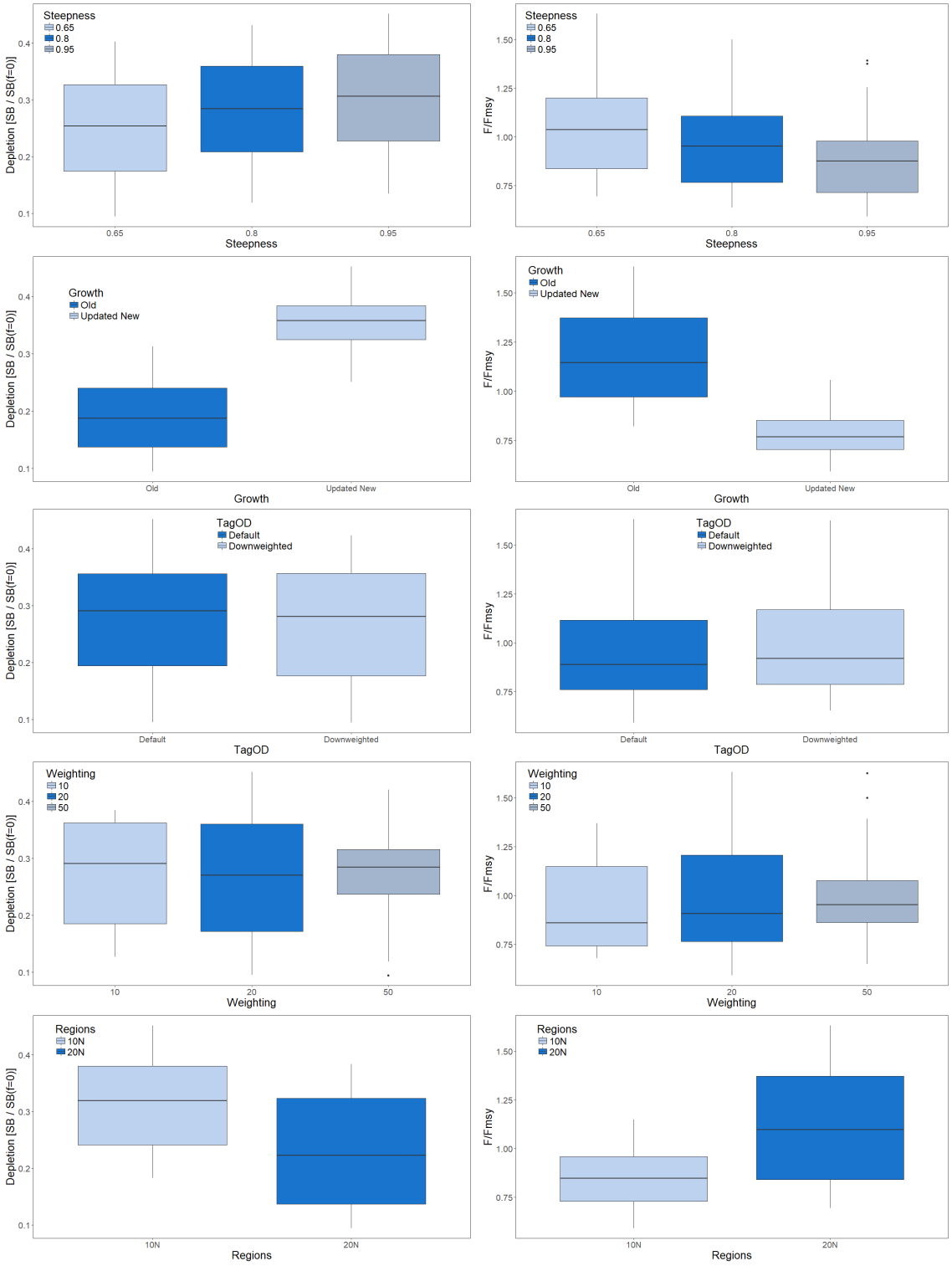

Figure 6: Boxplots summarizing the results of the structural uncertainty grid with respect to the spawning potential reference point $SB_{recent}/SB_{F=0}$ (left panels), and the fishing mortality reference point $F_{recent}/F_{\mathrm{MSY}}$ (right panels). The colors indicate the level of the model with respect to each uncertainty axis.

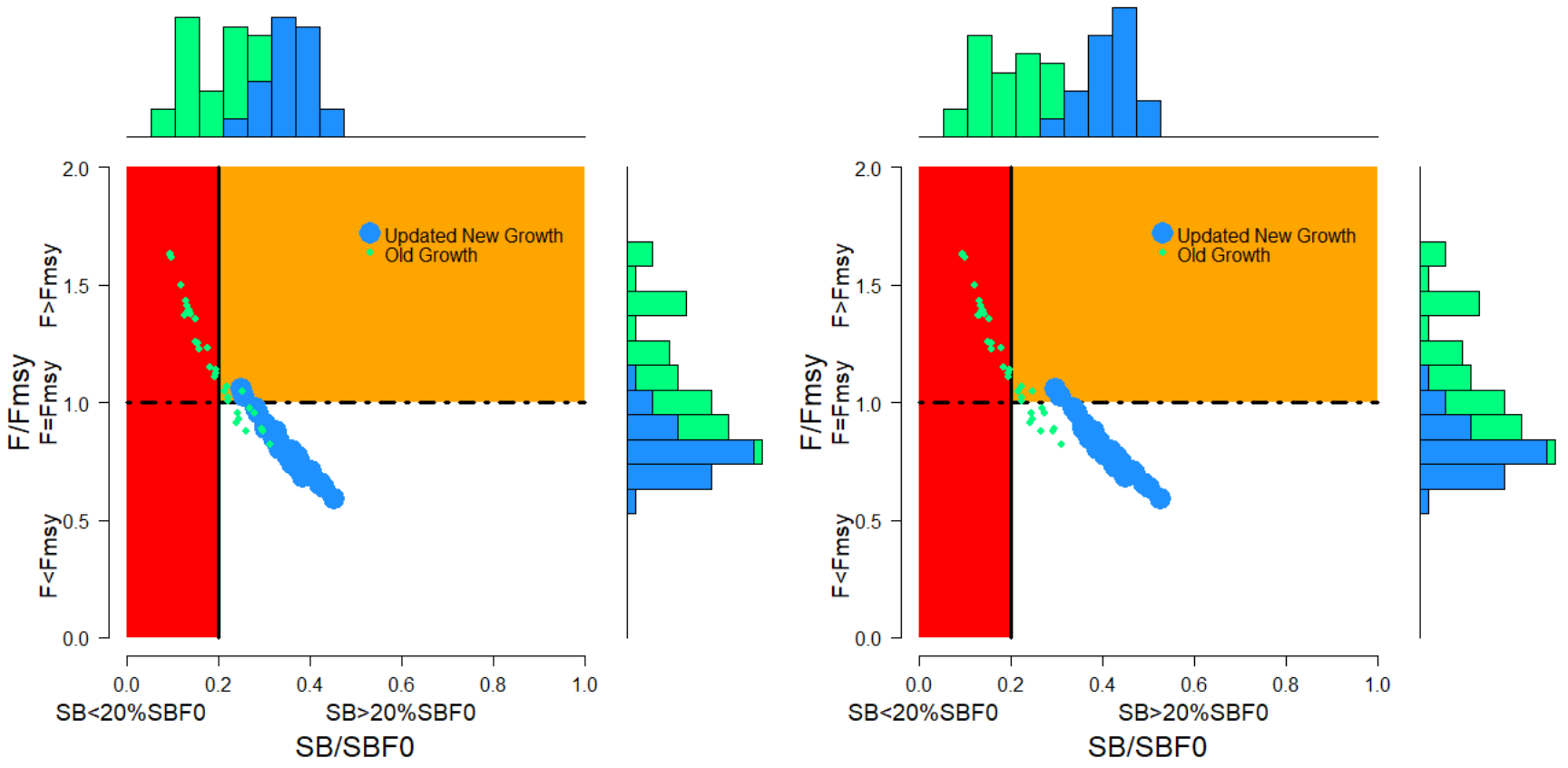

(a) $SB_{recent}/SB_{F=0}$ (b) $SB_{latest}/SB_{F=0}$

Figure 7: Majuro plots summarizing the results for each of the 72 models in the structural uncertainty grid, which are colored by the growth assumption for the reference point (a) $SB_{recent}/SB_{F=0}$ and (b) $SB_{latest}/SB_{F=0}$. The plots represent estimates of stock status in terms of spawning potential depletion and fishing mortality where the size of the circle is indicative of the weight in calculating the reference point table. The red zone represents spawning potential levels lower than the agreed limit reference point which is marked with the solid black line. The orange region is for fishing mortality greater than F_{MSY} (F_{MSY} is marked with the black dashed line).

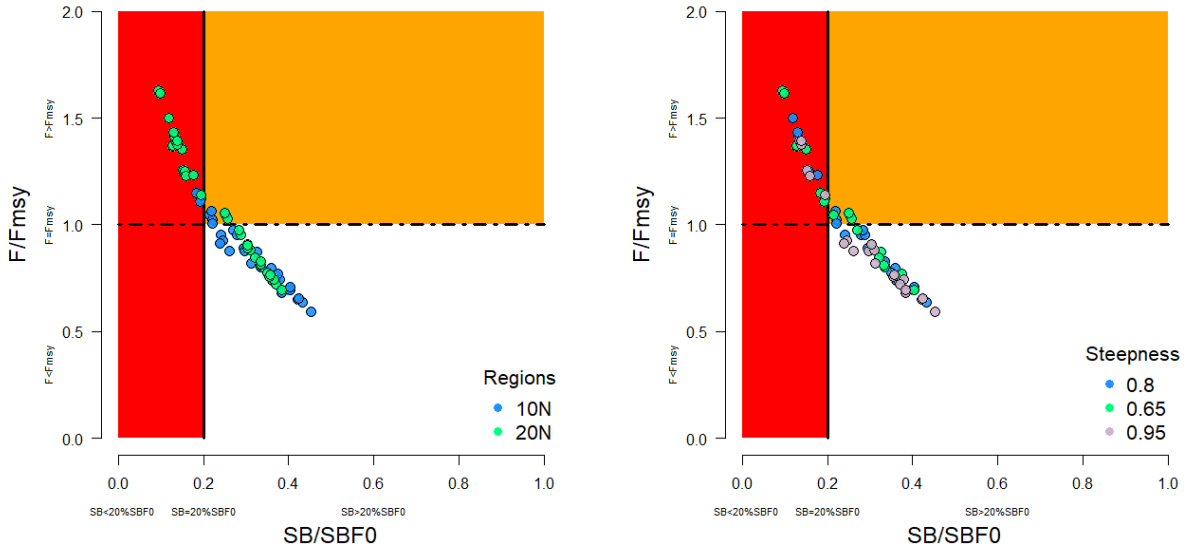

(a) 20° N and 10° N regions

(b) Steepness

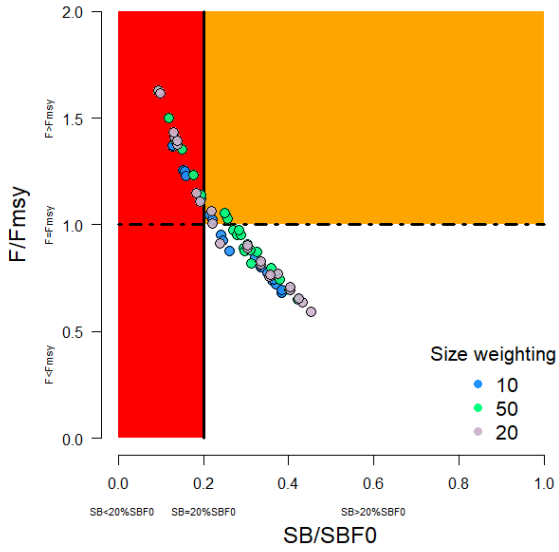

(c) Weighting of size data

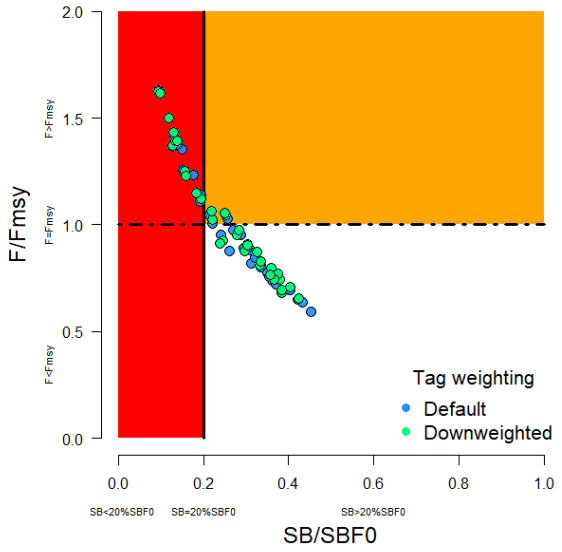

(d) Tagging data weighting

Figure 8: Majuro plots summarizing the results for each of the 72 models in the structural uncertainty grid. The plots represent estimates of stock status in terms of spawning potential depletion for the reference point $SB_{recent}/SB_{F=0}$ and fishing mortality. The red zone represents spawning potential levels lower than the agreed limit reference point which is marked with the solid black line. The orange region is for fishing mortality greater than F_{MSY} (F_{MSY} is marked with the black dashed line). Panels (a)–(d) show the estimates for the different levels for four of the axes of the grid.

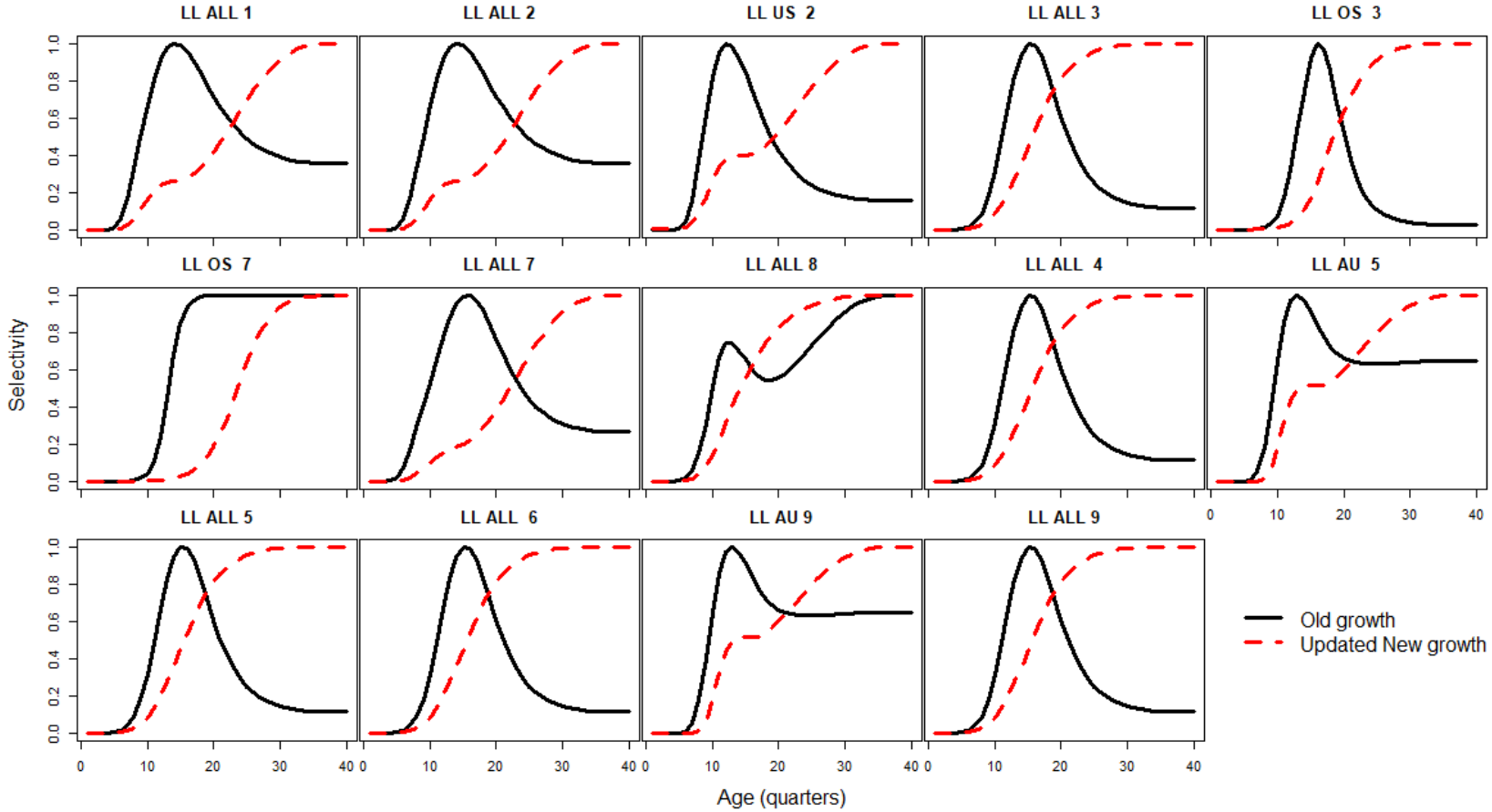

Figure 9: Estimated age-specific selectivity coefficients for the longline fisheries from models that assumed "Updated New growth" (red dashed line) or "Old growth" (black solid line).

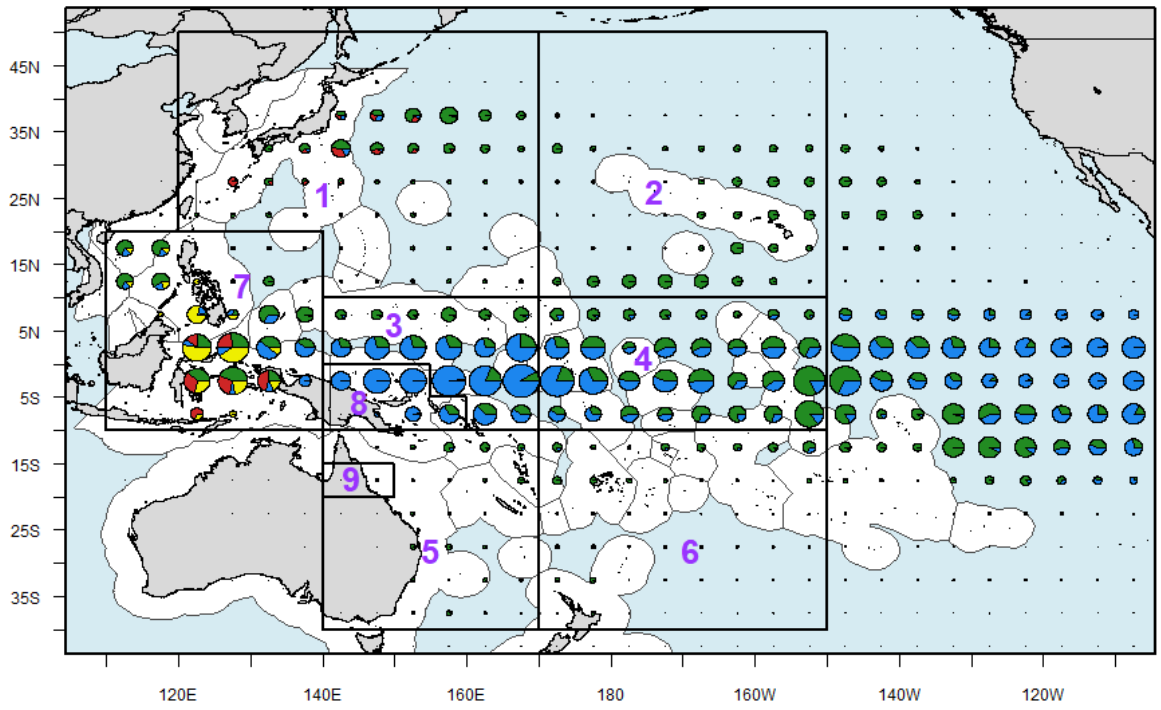

Figure 10: Distribution and magnitude of bigeye tuna catches for the most recent decade of the stock assessment (2006-2015) by 5° square and fishing gear: longline (green), pole-and-line (red), purse seine (blue) and miscellaneous (yellow), for the WCPO and part of the EPO. Overlaid are the regional boundaries for the stock assessment (10° N regional structure).

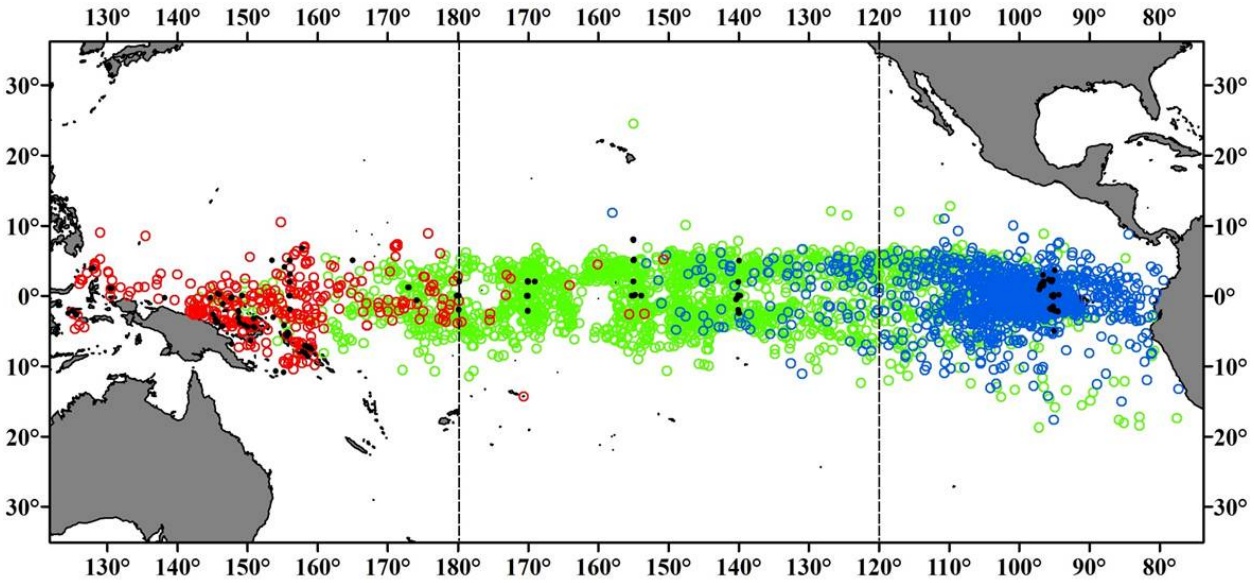

Figure 11: Map of the movements of tagged bigeye released in the Pacific Ocean and subsequently recaptured. The figure is sourced from Schaefer et al. (2015), and shows the three regions they split their data by. The small black points are the release locations, the red points are the recapture locations of fish released in the western region, the green points are the recapture locations of fish released in the central region and the blue points are the recapture locations of fish released in the eastern region.

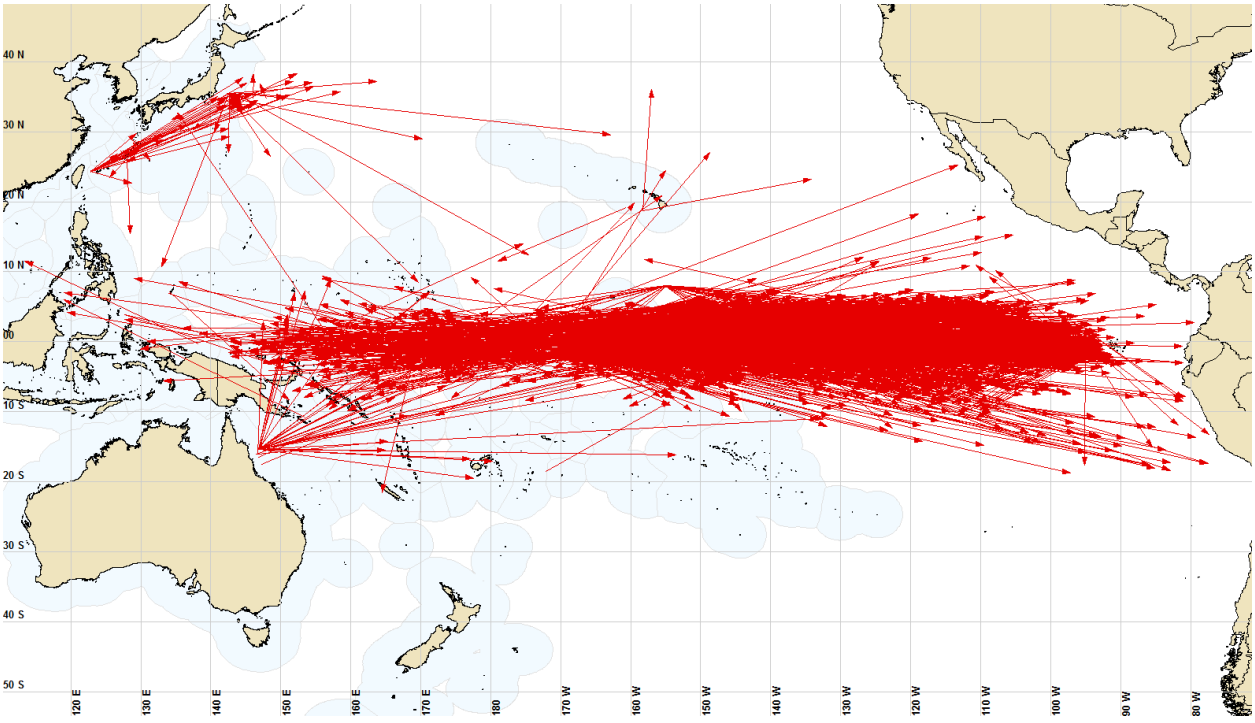

Figure 12: Map of the movements of tagged bigeye released in the Pacific Ocean and subsequently recaptured more than 1,000 nautical miles from their release site.

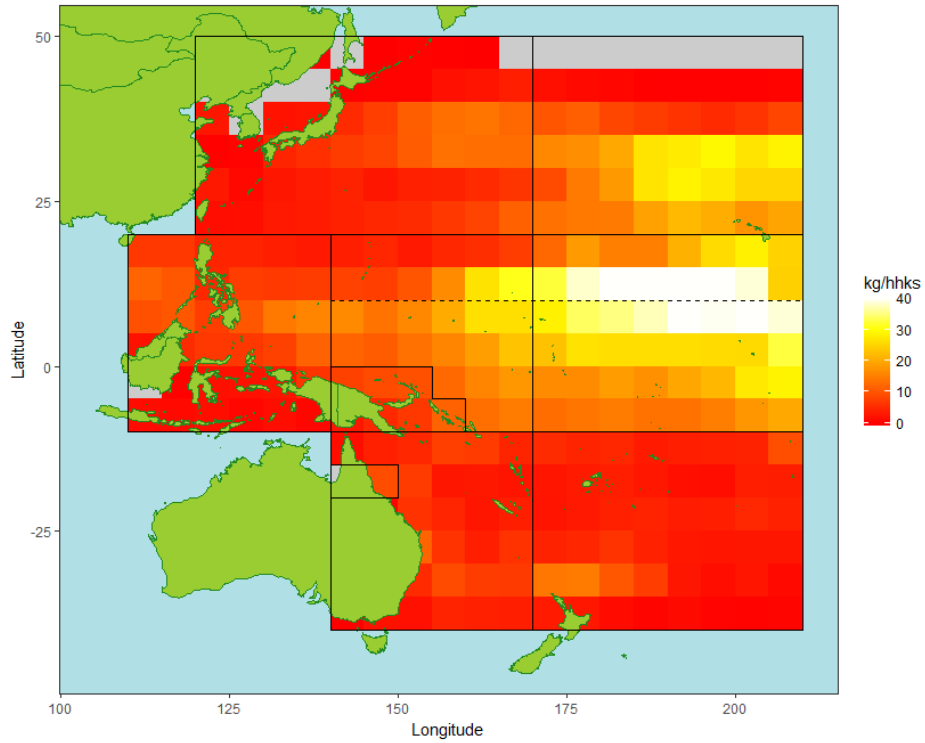

(a) Kilograms per hundred hooks

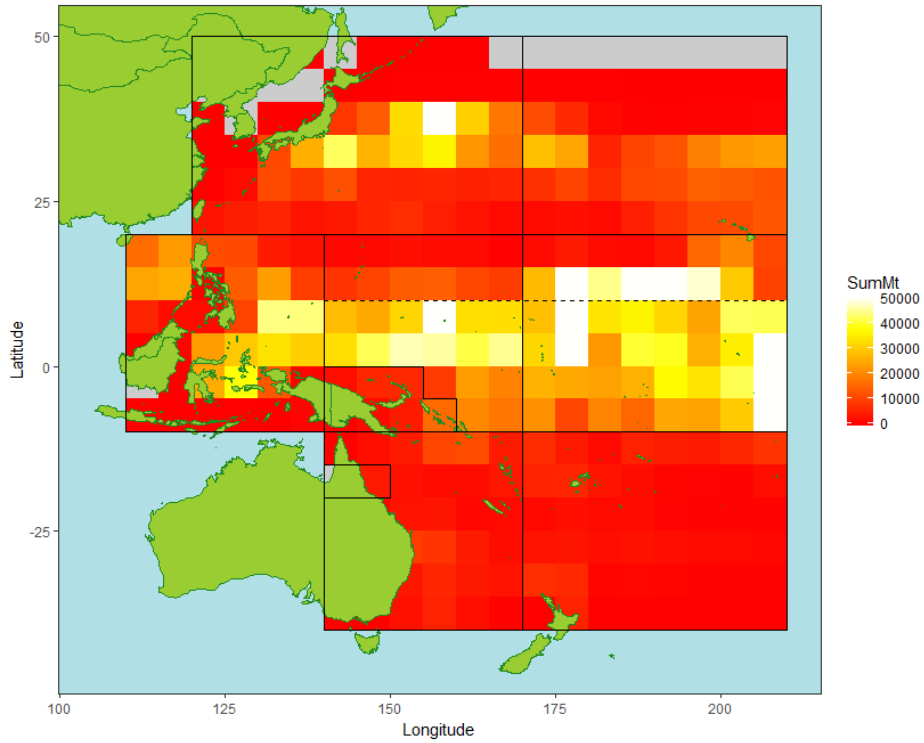

(b) Sum of metric tonnes

Figure 13: Heat maps for the bigeye longline fishery for the time period 1950 to 2017 of (a) average catch per unit effort (CPUE) in terms of kilograms per hundred hooks and (b) total catch in metric tonnes, where lighter colors indicate larger values and zeros are light gray. Regional boundaries for the 20° N structure are overlaid as a solid black line. The northern boundary of regions 3 and 4 for the 10° N spatial structure is shown as a dashed black line.

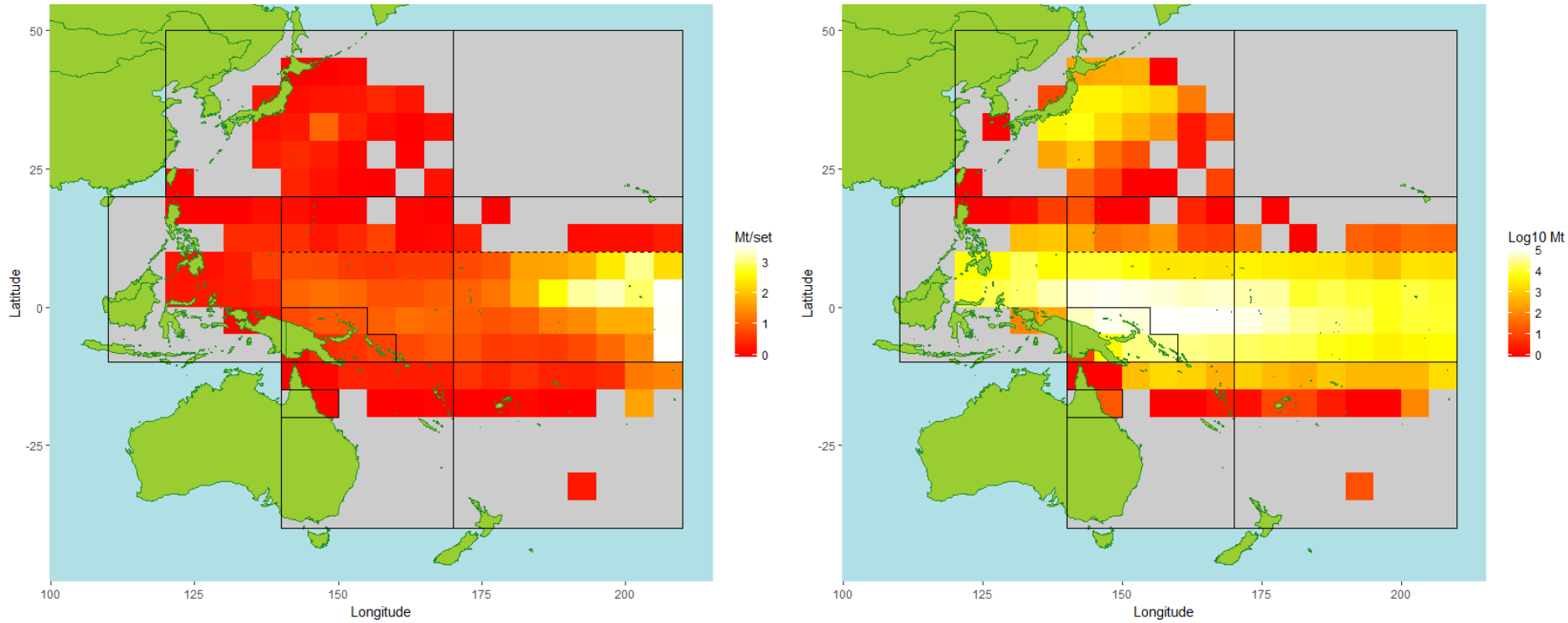

(a) Metric tonnes per set

(b) Sum of metric tonnes

Figure 14: Heat map for the bigeye purse seine fishery for the time period 1967 to 2017 of (a) average catch per unit effort (CPUE) in terms of metric tonnes per set and (b) log_{10} total catch in metric tonnes, where lighter colors indicate larger values and zeros are light gray. Regional boundaries for the 20° N structure are overlaid as a solid black line. The northern boundary of regions 3 and 4 for the 10° N spatial structure is shown as a dashed black line.

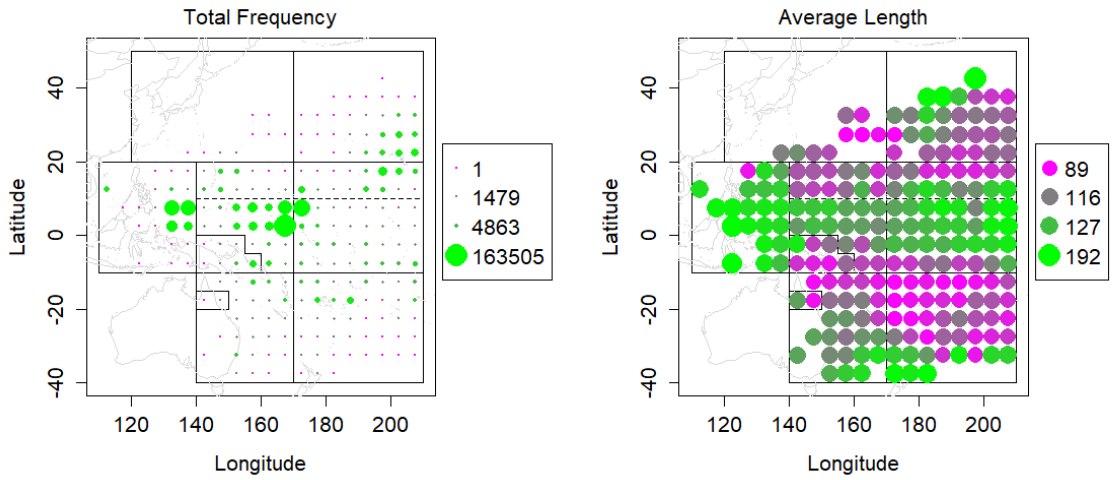

(a) Longline Fishery

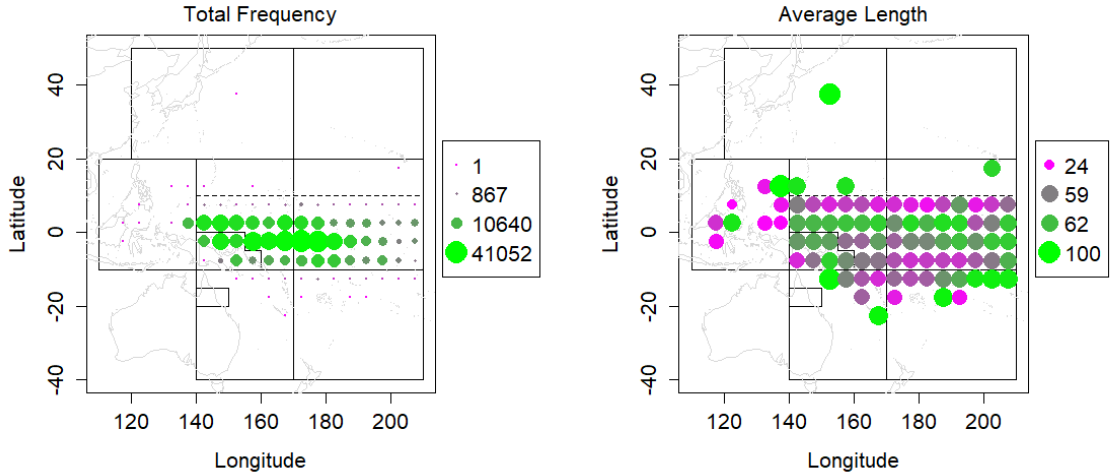

(b) Purse Seine Fishery

Figure 15: Average length of bigeye and total frequency of samples from the 5° x 5° sampling for (a) the longline fishery, and (b) the purse seine fishery.

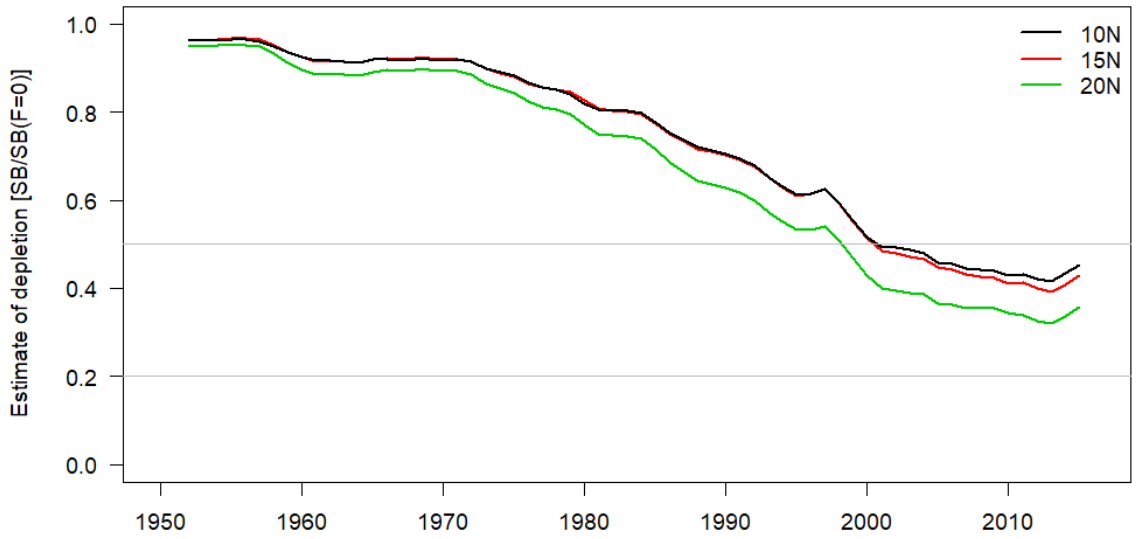

Figure 16: Estimated fishing depletion (of spawning potential) for three assessment models with the northern boundary of region 3 and 4 at 10° N, 15° N, and 20° N assuming the "Updated New growth", steepness of 0.8, default tagging overdispersion, and size composition weighting of 20 (see Section 4.3).

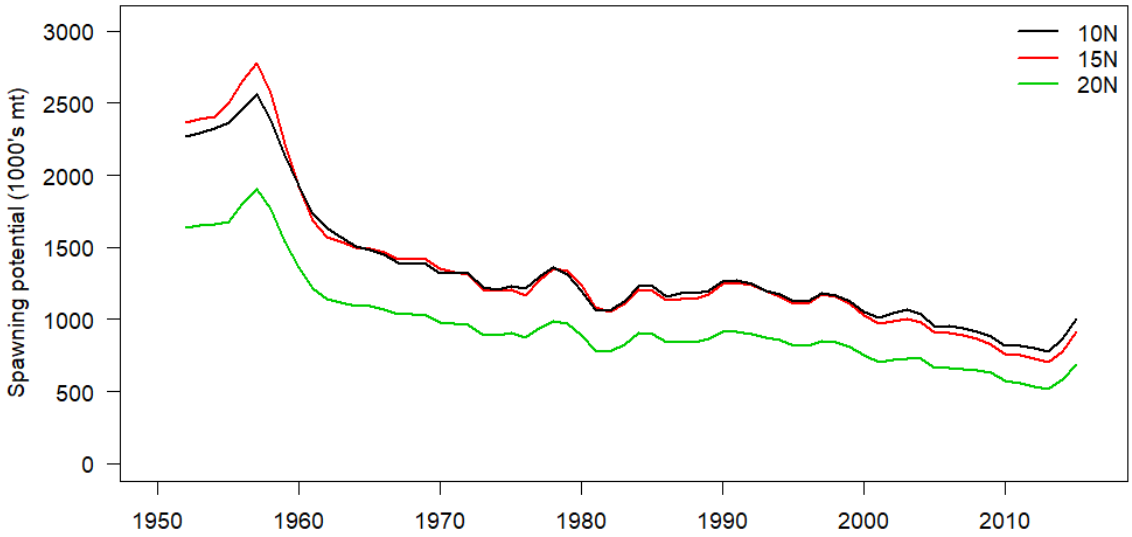

Figure 17: Estimated spawning potential for three assessment models with the northern boundary of region 3 and 4 at 10° N, 15° N, and 20° N assuming the "Updated New growth", steepness of 0.8, default tagging overdispersion, and size composition weighting of 20 (see Section 4.3).

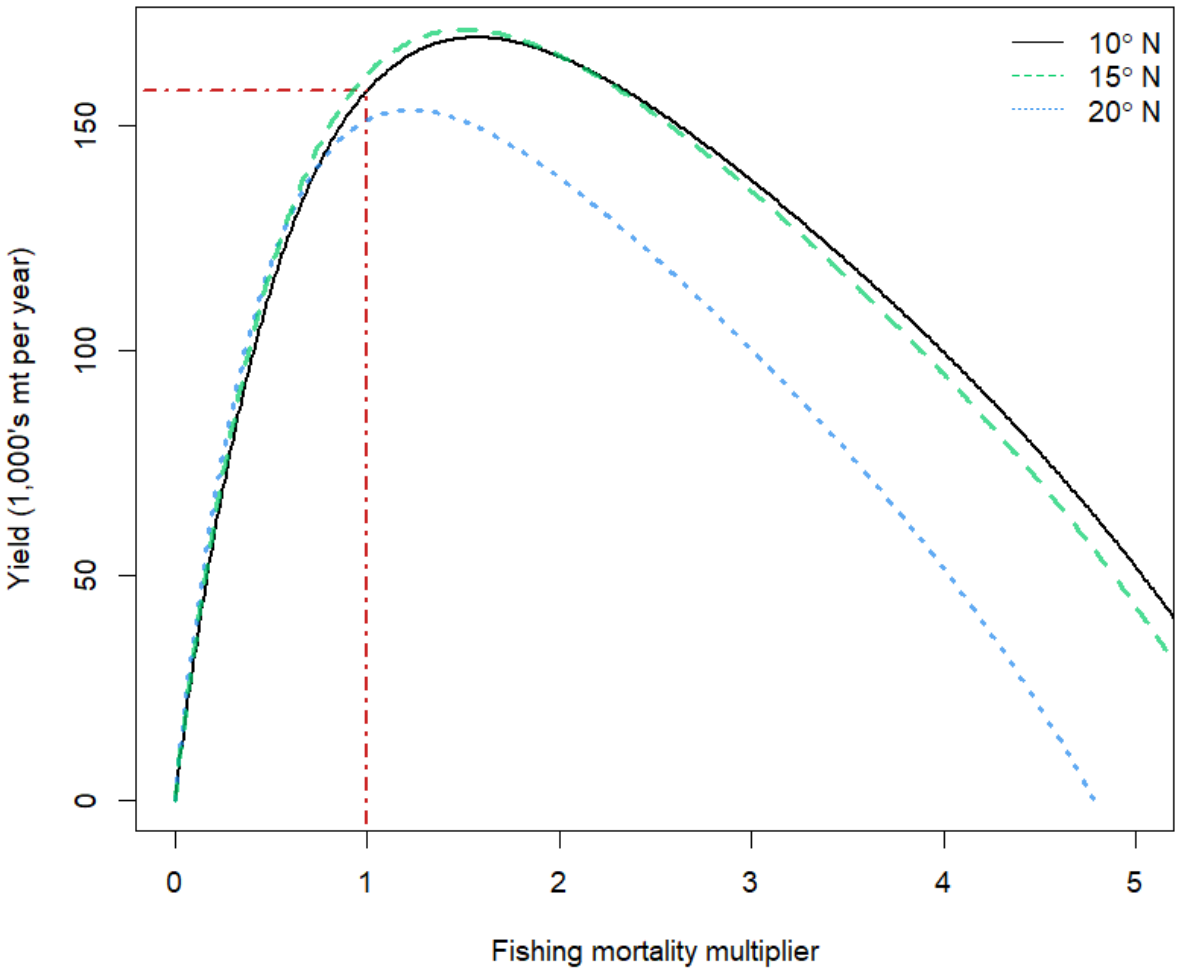

Figure 18: Estimated yield as a function of fishing mortality multiplier for three example models. The black line is the estimated yield curve for the 10° N model and the red dashed lines indicate the equilibrium yield at current fishing mortality. The yield curve for the 15° N model is displayed as the green dashed line and the 20° N model is displayed as the blue dotted line.

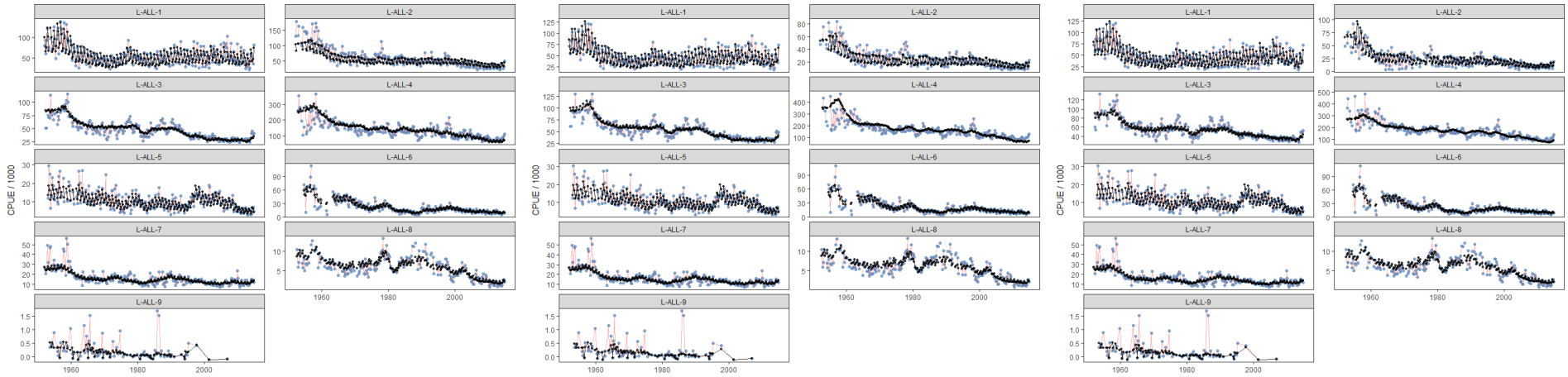

(a) 10° N (b) 15° N (c) 20° N

Figure 19: Observed (blue points and red lines) and model-predicted (black points and lines) CPUE for the eight fisheries which received standardised CPUE indices and the nominal CPUE index used for region 9 for models that assumed a northern bourndary of regions 3 and 4 at (a) 10° N, (b) 15° N, (c) and 20° N.

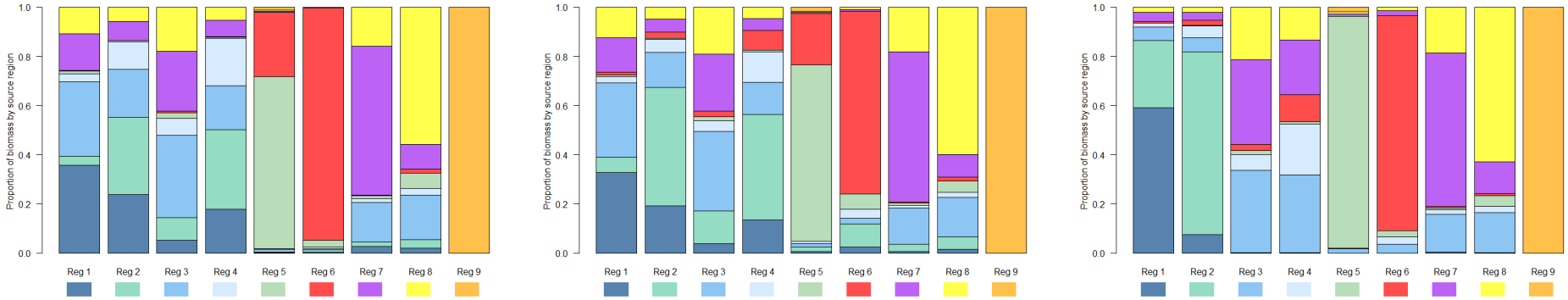

(a) 10° N (b) 15° N (c) 20° N

Figure 20: Proportional distribution of total biomass (by weight) in each region apportioned by the source region of the fish, for models that assume the northern boundary of regions 3 and 4 at (a) 10° N, (b) 15° N, and (c) 20° N. The colour of the home region is presented below the corresponding label on the x-axis. The biomass distributions are calculated based on the long-term average distribution of recruitment between regions, estimated movement parameters, and natural mortality.